

# AUGMENTED LAGRANGIAN PRECONDITIONERS FOR FICTITIOUS DOMAIN FORMULATIONS OF ELLIPTIC INTERFACE PROBLEMS

MICHELE BENZI, MARCO FEDER, LUCA HELTAI, AND FEDERICA MUGNAIONI

**ABSTRACT.** We present a novel augmented Lagrangian (AL) preconditioner for the solution of linear systems arising from finite element discretizations of elliptic interface problems with jump coefficients. The method is based on the Fictitious Domain with Distributed Lagrange Multipliers formulation and it is designed to improve the convergence of the Flexible Generalized Minimal Residual (FGMRES) method in the presence of large coefficient jumps. To reduce the computational cost, we also introduce a cheaper block-triangular variant of the preconditioner. We prove eigenvalue clustering for the ideal AL preconditioner and study the limiting behavior of the spectrum for the modified variant in terms of parameters and the size of the jumps. Numerical experiments on different immersed geometries confirm mesh-independent iteration counts and robustness over large coefficient jumps, with substantial reductions in wall-clock time for the modified approach.

*Keywords:* Preconditioning; Augmented Lagrangian method; Iterative solvers; Fictitious domain method; Elliptic interface problems; Non-matching meshes; Finite element method.

## 1. INTRODUCTION

In this work, we consider the efficient numerical solution of elliptic interface problems with discontinuous coefficients across an internal interface. Problems of this type arise in many scientific and engineering applications, including biosciences and fluid–structure interaction (FSI), where fluid and solid regions exhibit distinct physical properties across the interface.

A classical strategy to handle interface problems is to use *fitted approaches*, which involve generating a mesh that conforms to the interface between different materials or regions and provide accurate solutions [9, 48, 49, 54, 32]. In FSI, a prominent fitted strategy is the Arbitrary Lagrangian–Eulerian (ALE) approach [35, 46, 52], where compatibility between fluid and solid kinematics can be enforced by construction. In settings with large interface motion or deformation, however, maintaining mesh quality can require mesh-motion strategies and, in some cases, remeshing, which may increase computational cost, particularly in three-dimensional simulations. Motivated by these considerations, a range of *unfitted methods* have been developed over the past decades, where the computational mesh does not need to conform to the interface and the interface is permitted to cut through elements. Representative examples include the Immersed Boundary Method by Peskin [58], where the interface position is tracked by regularized Dirac delta distributions, and the level set method [64, 31], where the interface corresponds to the zero level set of a certain function. Other techniques, such as Nitsche-XFEM [1], Cut-FEM [29, 27, 28, 43], and Finite Cell methods [33, 34, 38] typically enforce interface/boundary conditions weakly via Nitsche-type couplings and/or stabilization terms. An alternative strategy is offered by the Fictitious Domain approach, spanning applications ranging from particulate flow simulations [39, 40] to more general cases considered in later works [18, 66]. Building on the idea of fictitiously extending one domain into the other, the method introduced in [21] proposes a new Fictitious Domain formulation with Distributed Lagrange Multipliers (FD-DLM) to address elliptic interface and FSI problems. The method employs independent meshes (one for the extended domain, and one for the immersed domain) that are generated only once and remain fixed throughout the computation. To enforce that the solutions coincide in both domains, a suitable coupling term is introduced, implemented through a distributed Lagrange multiplier.

Elliptic interface and FSI problems share the common feature of involving a domain split into two regions separated by an interface. In the former case, this separation is due to the presence of discontinuous coefficients, whereas in the latter it reflects the presence of two different equations, corresponding to constitutive models for the fluid and the solid.

Focusing on the elliptic interface case, the analysis of a fictitious domain-like approach using continuous finite elements was first introduced in [8], and more recently extended to discontinuous elements in [4]. Independently of the chosen discretization, the method leads to a saddle point problem with a  $3 \times 3$  block structure of this form:

$$(1) \quad \begin{bmatrix} \mathbf{A} & 0 & \mathbf{C}^\top \\ 0 & \mathbf{A}_2 & -\mathbf{C}_2^\top \\ \mathbf{C} & -\mathbf{C}_2 & 0 \end{bmatrix} \begin{bmatrix} \mathbf{u} \\ u_2 \\ \lambda \end{bmatrix} = \begin{bmatrix} \mathbf{f} \\ \mathbf{g} \\ 0 \end{bmatrix},$$

where  $\mathbf{A} \in \mathbb{R}^{n \times n}$  is symmetric positive definite (SPD),  $\mathbf{A}_2 \in \mathbb{R}^{m \times m}$  is symmetric positive *semidefinite* (SPSD),  $\mathbf{C} \in \mathbb{R}^{\ell \times n}$ , and  $\mathbf{C}_2 \in \mathbb{R}^{\ell \times m}$ .

This three-by-three block structure also appears, although with different meaning in terms of operators and unknowns, in a variety of application problems. In the context of PDE-constrained optimization and optimal control problems, suitable preconditioning strategies have been proposed in [13, 61, 62, 63, 57].

The system matrix in (1) can be regarded as a  $2 \times 2$  block matrix:

$$(2) \quad \mathcal{A} = \begin{bmatrix} \tilde{\mathbf{A}} & \mathbf{B}^\top \\ \mathbf{B} & 0 \end{bmatrix}, \quad \text{where } \tilde{\mathbf{A}} = \begin{bmatrix} \mathbf{A} & 0 \\ 0 & \mathbf{A}_2 \end{bmatrix} \quad \text{and } \mathbf{B} = [\mathbf{C} \quad -\mathbf{C}_2],$$

indicating that the problem is, in principle, amenable to a *standard* saddle point problem. For large discretizations (particularly in 3D), memory and factorization costs often make fully direct solution strategies impractical, motivating iterative Krylov methods with robust preconditioning. In addition, the resulting linear systems can become challenging for Krylov methods due to coefficient contrast, the semidefinite sub-block associated with the immersed-domain operator, and the multi-mesh coupling. These features can lead to severe ill-conditioning and, consequently, to a deterioration of the convergence rate. Therefore, designing a suitable preconditioner is crucial to accelerate the convergence of iterative methods and to guarantee robustness not only with respect to the mesh sizes, but also with respect to coefficient jumps across subdomains.

If  $\tilde{\mathbf{A}}$  were invertible, classical block preconditioners such as those surveyed in [12] could be considered. However, these approaches rely on the Schur complement  $\tilde{\mathbf{S}} = \mathbf{B}\tilde{\mathbf{A}}^{-1}\mathbf{B}^\top$ , and thus cannot be applied directly to (2), where  $\tilde{\mathbf{A}}$  is singular due to the semidefiniteness of  $\mathbf{A}_2$ . Moreover, strategies requiring an approximation of the Schur complement  $\mathbf{S} = \mathbf{C}\mathbf{A}^{-1}\mathbf{C}^\top$  (such as the ones in [62]) are especially challenging for unfitted methods; difficulties arise because the matrix  $\mathbf{C}$  in (1) involves products of basis functions defined on two arbitrarily overlapping grids [20, 22, 50], making it unclear to which matrix  $\mathbf{S}$  should be spectrally equivalent.

Preconditioners for fictitious domain formulations of elliptic interface problems have already been investigated, e.g. in [65], where an augmented Lagrangian (AL) Uzawa iterative method is presented. Reported results indicate robustness with respect to coefficient contrast, but iteration counts and parameter sensitivity remain non-trivial in some regimes. Later, in the context of FSI simulations, a block preconditioner was studied in [26] using sparse direct solvers for the inversion of diagonal blocks. Recently, an iterative version based on multigrid methodologies has been tested in [2] for the elliptic interface case. For the fictitious domain approach with boundary-supported Lagrange multipliers applied to Poisson and Stokes problems, a novel augmented Lagrangian preconditioner was recently proposed and analyzed by the authors in [11]. Originally developed for finite element discretizations of the Oseen problem arising from Picard linearizations of the steady Navier-Stokes equations [14, 37], augmented Lagrangian preconditioners effectively bypass the need for a good approximation of the dense Schur complement matrix. In the context of elliptic interface problems, an additional important benefit arises: the augmentation removes the singularity from the  $(2, 2)$ -block in (1). Motivated by these considerations, in this work we extend the results and preconditioning techniques presented in [11] to handle linear systems of equations arising from the fictitious domain formulation with distributed Lagrange multipliers for elliptic interface

problems. The resulting *ideal* AL preconditioner admits a spectral analysis showing favorable eigenvalue clustering and mesh-independent bounds; numerically we observe robust iteration counts over wide coefficient contrasts.

The term *ideal* refers to a theoretical formulation of the preconditioner where the action of inverses is assumed to be computed exactly. This is, however, impractical, due to its high computational cost. The main cost arises from the solution of linear systems with the augmented term, making efficient inexact solvers essential. A tailored geometric multigrid cycle used as an approximate solver for the velocity subproblem associated with the  $(1, 1)$ -block of the preconditioner in the AL formulation of the Oseen problem was initially proposed in [14], and later extended to three dimensions in [37], inspired by the multigrid framework presented in [60]. While this strategy yields optimal results in terms of iteration counts as well as robustness with respect to a wide range of Reynolds numbers, its implementation can be challenging for general discretizations and geometries. For this reason, a so-called *modified AL preconditioner* was introduced in [16] for the Oseen problem, whose block-triangular structure makes it easier to implement. In particular, off-the-shelf algebraic multigrid solvers for scalar elliptic PDEs can be employed to solve the subsystems arising during the application of the preconditioner, providing an efficient approach for inverting the diagonal blocks. A spectral analysis of this modified AL-based preconditioner was presented in [17], giving a recipe for the choice of the augmentation parameter  $\gamma$ . Since the augmented operator in our formulation couples two overlapping grids, constructing a monolithic geometric multigrid solver is challenging; we therefore adopt a modified AL strategy that admits efficient sub-solves using standard Algebraic MultiGrid (AMG) components.

Summarizing, the main contributions of our work are the following. First, we develop a novel augmented Lagrangian preconditioner for the fictitious domain (FD-DLM) formulation of elliptic interface problems, which demonstrates robustness and low iteration counts across a wide range of problem regimes. Second, we introduce a computationally efficient modified variant of this preconditioner that leverages standard algebraic multigrid solvers for the diagonal blocks, significantly reducing implementation complexity and overall time-to-solution. Third, we provide a rigorous spectral analysis, demonstrating favorable eigenvalue clustering and robustness with respect to large coefficient jumps across the interface. Finally, we present extensive numerical validation of the proposed preconditioners, including challenging three-dimensional problems in linear elasticity with heterogeneous material properties.

We point out that one important reason for studying efficient preconditioners for the elliptic interface problem with a Lagrange multiplier formulation lies in the fact that its block structure naturally arises as a sub-block of a  $4 \times 4$  block system obtained when using a monolithic formulation for the FSI problem with Lagrange multipliers, where additional blocks of such a system are related to the incompressibility constraint of the fluid. As proven in [30], monolithic schemes for FSI do not suffer from the so-called *added mass effect* when the densities of fluid and solid bodies are comparable, as it is the case in the context of biological tissues. The conditioning of the system arising from FD-DLM applied to the monolithic FSI problem was recently analyzed in [24].

The paper is organized as follows. In Section 2, we present the FD-DLM formulation for a generic elliptic interface problem, describe the finite element discretization, recall existence and uniqueness results, and derive the resulting saddle-point system. In Section 3, we derive the ideal augmented Lagrangian preconditioner for our model problem, while Section 4 is devoted to its spectral analysis. In Section 5, we introduce a modified variant of the ideal AL preconditioner, which is easier to implement and more efficient in practice. Its spectral analysis is presented in Section 6. Section 7 presents several numerical experiments to validate the proposed preconditioners, demonstrating their robustness and effectiveness for various problem configurations, including cases with large coefficient jumps. We conclude our experiments by applying the preconditioner to a three-dimensional linear elasticity problem with heterogeneous material properties characterized by different Lamé constants in each subdomain. Finally, in Section 8, we summarize our main results and identify avenues for future research.

## 2. ELLIPTIC INTERFACE PROBLEM AND FICTITIOUS DOMAIN APPROACH

**2.1. Notation.** We start by fixing some notation. Given an open and bounded domain  $D$ , we denote with  $L^2(D)$  the space of square integrable functions on  $D$ , endowed with the norm  $\|\cdot\|_{0,D}$  induced by the inner

product  $(\cdot, \cdot)_D$ . Sobolev spaces are denoted by  $W^{s,p}(D)$ , where  $s \in \mathbb{R}$  refers to the differentiability index and  $p \in [1, \infty]$  is the integrability exponent. In the case  $p = 2$ , we use the notation  $H^s(D) = W^{s,2}(D)$ , with associated norm  $\|\cdot\|_{s,D}$  and seminorms  $|\cdot|_{s,D}$ . We use normal font, e.g.  $A$ , to denote linear operators, while matrices and vectors are denoted by the sans serif font, e.g.  $\mathbf{A}$  and  $\mathbf{x}$ , respectively. A calligraphic font, e.g.  $\mathcal{A}$ , is used to denote block matrices associated with saddle point systems. The spectrum of a matrix is denoted by  $\text{Spec}(\cdot)$ . Finally, we will use the letter  $\lambda$  to denote both the Lagrange multiplier of our weak formulation, and the generic eigenvalue of a matrix. The different meaning will be clear from the context, and no confusion should arise.

**2.2. Elliptic interface problem.** Let  $\Omega$  be a domain in  $\mathbb{R}^d$ , where  $d \in \{2, 3\}$ , with a bounded Lipschitz boundary  $\partial\Omega$ . Let  $\Omega_1$  and  $\Omega_2$  be two subdomains of  $\Omega$  such that  $\overline{\Omega} = \overline{\Omega_1} \cup \overline{\Omega_2}$ , and let the interface  $\Gamma = \overline{\Omega_1} \cap \overline{\Omega_2}$  be Lipschitz continuous. We call  $\Omega$  the *background domain* and  $\Omega_2$  the *immersed domain*, which we assume to be entirely contained in  $\Omega$ , i.e.  $\overline{\Gamma} \cap \partial\Omega = \emptyset$ .

We consider the following *elliptic interface problem* with a jump in the coefficients.

**Problem 1.** For  $i = 1, 2$ , given forcing terms  $f_i: \Omega_i \rightarrow \mathbb{R}$ , and positive coefficients  $\beta_i \in L^\infty(\Omega_i)$ , find  $u_1: \Omega_1 \rightarrow \mathbb{R}$  and  $u_2: \Omega_2 \rightarrow \mathbb{R}$  such that:

$$(3) \quad \begin{cases} -\operatorname{div}(\beta_i \nabla u_i) = f_i & \text{in } \Omega_i, \\ u_1 = u_2 & \text{on } \Gamma, \\ \beta_1 \nabla u_1 \cdot \mathbf{n}_1 = -\beta_2 \nabla u_2 \cdot \mathbf{n}_2 & \text{on } \Gamma, \\ u_1 = 0 & \text{on } \partial\Omega_1. \end{cases}$$

In the above problem,  $\mathbf{n}_i$  ( $i = 1, 2$ ) denotes the unit vector normal to  $\Gamma$ , pointing out of  $\Omega_i$ . The two transmission conditions on  $\Gamma$  enforce the continuity of  $u_1$  and  $u_2$ , as well as the continuity of the co-normal derivatives on the interface. In 2D, this model describes the displacement of a membrane made of two different materials. We assume the coefficients to be bounded by positive constants  $\beta_1$  and  $\beta_2$ , i.e.,  $\beta_1 > \beta_1 > 0$  and  $\beta_2 > \beta_2 > 0$ . Such coefficients  $\beta_i$  may represent the stiffness of such materials,  $f_i$  the loads applied to the membrane, and  $u_i$  the vertical displacement in  $\Omega_i$ , respectively. Notably, the condition  $u_1 = u_2$  on  $\Gamma$  implies that the materials are perfectly bonded. For the sake of simplicity, we will assume  $\beta_1$  and  $\beta_2$  to be positive constants throughout the paper, although the proposed approach can be extended to variable coefficients without significant modifications.

In this paper, we consider a fictitious domain reformulation of Problem 1, following [8]. In detail, we extend  $\beta_1$  and  $f_1$ , originally defined in  $\Omega_1$ , to the whole  $\Omega$ . We denote the corresponding extensions with  $\beta$  and  $f$ , respectively, so that  $\beta|_{\Omega_1} = \beta_1$  and  $f|_{\Omega_1} = f_1$ . Similarly,  $u$  will denote the extension of  $u_1$  to  $\Omega$ , satisfying  $u|_{\Omega_1} = u_1$ . The extended solution  $u$  is then required to match  $u_2$  in the immersed domain  $\Omega_2$ . A graphical representation of such procedure is shown in Figure 1.

The condition  $u|_{\Omega_2} = u_2$  is enforced at the variational level by introducing the functional space  $\Lambda$  and a bilinear form  $c: \Lambda \times H^1(\Omega_2) \rightarrow \mathbb{R}$ , satisfying

$$c(\mu, v_2) = 0 \quad \forall \mu \in \Lambda \implies v_2 = 0 \quad \text{in } \Omega_2.$$

In this work, we consider  $\Lambda = H^{-1}(\Omega_2)$ , the dual space of  $H^1(\Omega_2)$ , and  $c(\mu, v_2) = \langle \mu, v_2 \rangle$ , the duality pairing between  $H^{-1}(\Omega_2)$  and  $H^1(\Omega_2)$ , but other definitions for  $\Lambda$  and hence for  $c(\cdot, \cdot)$  are possible [3]. On the space  $\Lambda$ , we consider the usual dual norm

$$\|\mu\|_\Lambda = \sup_{v_2 \in V_2} \frac{\langle \mu, v_2 \rangle}{\|v_2\|_{1,\Omega_2}}.$$

Finally, the condition  $u|_{\Omega_2} = u_2$  is imposed by introducing a Lagrange multiplier  $\lambda \in \Lambda$  as unknown in the following weak formulation of Problem 1.

**Problem 2.** Given  $f \in L^2(\Omega)$  and  $f_2 \in L^2(\Omega_2)$ ,  $\beta \in L^\infty(\Omega)$  and  $\beta_2 \in L^\infty(\Omega_2)$ , find  $(u, u_2, \lambda) \in V \times V_2 \times \Lambda$  such that

$$(4) \quad (\beta \nabla u, \nabla v)_\Omega + c(\lambda, v|_{\Omega_2}) = (f, v)_\Omega \quad \forall v \in V := H_0^1(\Omega),$$

$$(5) \quad ((\beta_2 - \beta) \nabla u_2, \nabla v_2) - c(\lambda, v_2) = (f_2 - f, v_2)_{\Omega_2} \quad \forall v_2 \in V_2 := H^1(\Omega_2),$$

$$(6) \quad c(\mu, u|_{\Omega_2} - u_2) = 0 \quad \forall \mu \in \Lambda := H^{-1}(\Omega_2).$$

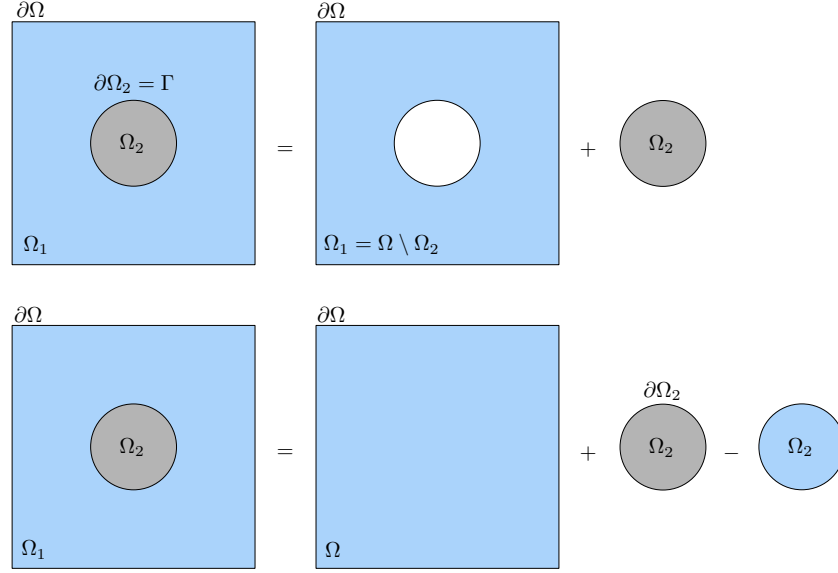


FIGURE 1. Top row: the initial configuration for Problem 1, involving the domains  $\Omega_1$  and  $\Omega_2$ . Bottom row: the fictitious domain reformulation, where the immersed domain  $\Omega_2$  is superimposed on  $\Omega$ . The solution  $u$  is defined in the whole  $\Omega$ , while  $u_2$  is defined only in  $\Omega_2$ . The fictitious contribution is then subtracted at the variational level *on the domain*  $\Omega_2$ .

The fictitious domain formulation in Problem 2 is equivalent to the original Problem 1 (details can be found in [8]). In operator matrix form, the weak formulation can be written as follows:

$$(7) \quad \begin{pmatrix} A & 0 & C^T \\ 0 & A_2 & -C_2^T \\ C & -C_2 & 0 \end{pmatrix} \begin{pmatrix} u \\ u_2 \\ \lambda \end{pmatrix} = \begin{pmatrix} F \\ G \\ 0 \end{pmatrix},$$

where  $A$  and  $A_2$  are the operators associated with bilinear forms  $(\beta \nabla u, \nabla v)_\Omega$  and  $((\beta_2 - \beta) \nabla u_2, \nabla v_2)_{\Omega_2}$ , respectively, while  $(C, -C_2)$  is the operator pair associated with  $c(\mu, u|_{\Omega_2} - u_2)$ , which has kernel

$$\mathbb{K} = \{(v, v_2) \in V \times V_2 : c(\mu, v|_{\Omega_2} - v_2) = 0 \quad \forall \mu \in \Lambda\}.$$

We now collect some basic facts about existence and uniqueness for this saddle point problem.

**Proposition 1** ([8], Prop. 1). *Given  $f \in L^2(\Omega)$  and  $f_2 \in L^2(\Omega_2)$ , Problem 2 has a unique solution  $(u, u_2, \lambda) \in V \times V_2 \times \Lambda$  such that the following estimate holds:*

$$(8) \quad \|u\|_{1,\Omega} + \|u_2\|_{1,\Omega_2} + \|\lambda\|_\Lambda \leq C (\|f\|_{0,\Omega} + \|f_2\|_{0,\Omega_2}),$$

where  $C$  is a positive constant.

The well-posedness of the saddle point Problem 2 follows from the fulfillment of the following sufficient conditions [19]. Proofs can be found in [4, 8].

- **Ellipticity on the kernel.** There exists a constant  $\hat{\alpha} > 0$  such that

$$(9) \quad (\beta \nabla v, \nabla v)_\Omega + ((\beta_2 - \beta) \nabla v_2, \nabla v_2)_{\Omega_2} \geq \hat{\alpha} (\|v\|_{1,\Omega}^2 + \|v_2\|_{1,\Omega_2}^2) \quad \forall (v, v_2) \in \mathbb{K}.$$

- **Inf-sup condition.** There exists a constant  $\hat{\theta} > 0$  such that

$$(10) \quad \sup_{(v,v_2) \in V \times V_2} \frac{c(\mu, v|_{\Omega_2} - v_2)}{(\|v\|_{1,\Omega}^2 + \|v_2\|_{1,\Omega_2}^2)^{\frac{1}{2}}} \geq \hat{\theta} \|\mu\|_\Lambda \quad \forall \mu \in \Lambda.$$

**2.3. Finite element discretization.** Problem 2 is discretized by mixed finite elements. We employ two *independent* and quasi-uniform meshes for  $\Omega$  and  $\Omega_2$  which we denote with  $\mathcal{T}_h$  and  $\mathcal{T}_{2,h}$ , respectively. We denote by  $h_\Omega$  the size of  $\mathcal{T}_h$ , and with  $h_{\Omega_2}$  the size of  $\mathcal{T}_{2,h}$ . In practice, we will choose the mesh sizes  $h_{\Omega_2}$  and  $h_\Omega$  to be approximately equal, so that their ratio is controlled and close to one. It is customary in fictitious domain approaches to have the background domain as a structured discretization of a  $d$ -dimensional box. Moreover, for a generic element  $K \in \mathcal{T}_h$  or  $\mathcal{T}_{2,h}$ , we define  $\mathcal{Q}^p(K)$ ,  $p \geq 1$ , to be the space of polynomials defined on  $K$  of degree at most  $p$  in each variable.

The finite element spaces are defined as follows:  $V_h \subset H_0^1(\Omega)$ ,  $V_{2,h} \subset H^1(\Omega_2)$ , and  $\Lambda_h \subset \Lambda$ . At the discrete level, if  $\Lambda_h \subset L^2(\Omega_2)$ , the duality pairing between  $\Lambda$  and its dual can be evaluated using the usual scalar product in  $L^2(\Omega_2)$ . Hence,

$$c(\mu_h, v_{2,h}) = (\mu_h, v_{2,h})_{\Omega_2} \quad \forall \mu_h \in \Lambda_h, \quad \forall v_{2,h} \in V_{2,h}.$$

All in all, the discrete formulation of Problem 2 reads as follows.

**Problem 3.** Given  $f \in L^2(\Omega)$  and  $f_2 \in L^2(\Omega_2)$ , find  $(u_h, u_{2,h}, \lambda_h) \in V_h \times V_{2,h} \times \Lambda_h$  such that

$$(11) \quad \begin{aligned} (\beta \nabla u_h, \nabla v_h)_\Omega + (\lambda_h, v_h|_{\Omega_2})_{\Omega_2} &= (f, v_h)_\Omega & \forall v_h \in V_h, \\ ((\beta_2 - \beta) \nabla u_{2,h}, \nabla v_{2,h})_{\Omega_2} - (\lambda_h, v_{2,h})_{\Omega_2} &= (f_2 - f, v_{2,h})_{\Omega_2} & \forall v_{2,h} \in V_{2,h}, \\ (\mu_h, u_h|_{\Omega_2} - u_{2,h})_{\Omega_2} &= 0 & \forall \mu_h \in \Lambda_h. \end{aligned}$$

In the following, we recall the discrete counterparts of conditions (9) and (10), which will be needed for the spectral analysis of the preconditioner. The ellipticity on the kernel is satisfied when  $\beta_2 > \beta > \bar{\beta} > 0$ , although the numerical findings reported in [4] suggest that this assumption might be relaxed. We first need to introduce the discrete kernel of  $c(\cdot, \cdot)$ :

$$\mathbb{K}_h = \{(v_h, v_{2,h}) \in V_h \times V_{2,h} : (\mu_h, v_h|_{\Omega_2} - v_{2,h})_{\Omega_2} = 0 \quad \forall \mu_h \in \Lambda_h\}.$$

The next two propositions ensure existence and uniqueness of the discrete solution to Problem 3. Thanks to these conditions, the theory of saddle point problems yields the usual quasi-optimal error estimate (cfr. [19, Th. 5.2.2]). Proofs of Propositions 2 and 3, which depend on the choice of finite dimensional subspaces, can be found in [4, 8]. Indeed, to solve Problem 3, a classical choice is to use continuous linear elements  $\mathcal{Q}^1$  for all the variables:

$$\begin{aligned} V_h &= \{v_h \in H_0^1(\Omega) : v_h|_K \in \mathcal{Q}^1(K) \text{ for all } K \in \mathcal{T}_h\} \subset H_0^1(\Omega), \\ V_{2,h} &= \{v_{2,h} \in H^1(\Omega_2) : v_{2,h}|_K \in \mathcal{Q}^1(K) \text{ for all } K \in \mathcal{T}_{2,h}\} \subset H^1(\Omega_2), \\ \Lambda_h &= V_{2,h}. \end{aligned}$$

Other stable choices satisfying the discrete inf-sup condition are also possible, such as  $\mathcal{Q}^2 - \mathcal{Q}^2 - \mathcal{Q}^0$  or  $\mathcal{Q}^1 - (\mathcal{Q}^1 + \mathfrak{B}) - \mathcal{Q}^0$ , where  $\mathcal{Q}^1 + \mathfrak{B}$  denotes the enrichment of  $\mathcal{Q}^1$  elements with bubble functions defined on each element  $K$  and vanishing on  $\partial K$  (see Remark 2).

**Proposition 2** (Discrete ellipticity on the kernel). *Let us consider  $V_h, V_{2,h}$  and  $\Lambda_h$  as defined above, and assume that  $\beta_2 > \beta > \bar{\beta} > 0$  in  $\Omega_2$ . Then, there exists a constant  $\alpha > 0$ , independent of the discretization parameters  $h_\Omega$  and  $h_{\Omega_2}$  such that for all  $(v_h, v_{2,h}) \in \mathbb{K}_h$ , the following inequality holds true.*

$$(12) \quad (\beta \nabla v_h, \nabla v_h)_\Omega + ((\beta_2 - \beta) \nabla v_{2,h}, \nabla v_{2,h})_{\Omega_2} \geq \alpha (|v_h|_{1,\Omega}^2 + \|v_{2,h}\|_{1,\Omega_2}^2).$$

**Proposition 3** (Discrete inf-sup condition). *Let  $V_h, V_{2,h}$  and  $\Lambda_h$  as defined above. Then, there exists a constant  $\theta > 0$ , independent of the discretization parameters  $h_\Omega$  and  $h_{\Omega_2}$ , such that the following inf-sup condition holds:*

$$(13) \quad \sup_{(v_h, v_{2,h}) \in V_h \times V_{2,h}} \frac{(\mu_h, v_h|_{\Omega_2} - v_{2,h})_{\Omega_2}}{(|v_h|_{1,\Omega}^2 + \|v_{2,h}\|_{1,\Omega_2}^2)^{\frac{1}{2}}} \geq \theta \|\mu_h\|_\Lambda \quad \forall \mu_h \in \Lambda_h.$$

We denote by  $\{\varphi_i\}_{i=1}^n$ ,  $\{\phi_j\}_{j=1}^m$ , and  $\{\psi_k\}_{k=1}^\ell$  the basis functions of  $V_h, V_{2,h}$  and  $\Lambda_h$ . The finite element discretization of Problem 3 yields the following linear system of  $(n + m + l) \times (n + m + l)$  equations for

$(\mathbf{u}, \mathbf{u}_2, \lambda)$

$$(14) \quad \begin{bmatrix} \mathbf{A} & 0 & \mathbf{C}^\top \\ 0 & \mathbf{A}_2 & -\mathbf{C}_2^\top \\ \mathbf{C} & -\mathbf{C}_2 & 0 \end{bmatrix} \begin{bmatrix} \mathbf{u} \\ \mathbf{u}_2 \\ \lambda \end{bmatrix} = \begin{bmatrix} \mathbf{f} \\ \mathbf{g} \\ 0 \end{bmatrix},$$

where

$$(15) \quad \begin{aligned} (\mathbf{A})_{i,j} &= \int_{\Omega} \beta \nabla \varphi_i \cdot \nabla \varphi_j, & (\mathbf{A}_2)_{i,j} &= \int_{\Omega_2} (\beta_2 - \beta) \nabla \phi_i \cdot \nabla \phi_j, \\ (\mathbf{C})_{i,k} &= (\psi_k, \varphi_i)_{\Omega_2} = \int_{\Omega_2} \psi_k \varphi_i, & (\mathbf{C}_2)_{k,j} &= (\phi_j, \psi_k)_{\Omega_2} = \int_{\Omega_2} \psi_k \phi_j, \\ (\mathbf{f})_i &= (f, \varphi_i)_{\Omega} = \int_{\Omega} f \varphi_i, & (\mathbf{g})_j &= (f_2 - f, \phi_j)_{\Omega_2} = \int_{\Omega_2} (f_2 - f) \phi_j. \end{aligned}$$

Notice that choosing  $V_{2,h} \equiv \Lambda_h$  implies that the basis functions for the multiplier space  $\Lambda_h$  coincide with those for  $V_{2,h}$ , that is,  $\{\psi_k\}_{k=1}^m = \{\phi_j\}_{j=1}^m$ . In this particular case, the matrix  $\mathbf{C}_2$  coincides with the mass matrix defined on the multiplier space  $\Lambda_h$ , whose generic entry is

$$(16) \quad (\mathbf{M})_{i,j} := (\psi_i, \psi_j)_{\Omega_2} = \int_{\Omega_2} \psi_i \psi_j.$$

**Remark 1** (Singularity of  $\mathbf{A}_2$ ). *Due to the lack of boundary conditions on  $\Omega_2$ , the discretization with finite elements of the bilinear form  $A_2$  will result in a singular matrix. More precisely, it coincides with the matrix of the pure Neumann problem defined on  $\Omega_2$ , for which the solution is unique up to an additive constant and hence  $\ker(\mathbf{A}_2) = \text{span}\{1\}$ . This does not imply that the resulting linear system of equations is singular, but poses significant challenges in the construction of a preconditioner.*

**Remark 2** (Other mixed discretizations). *Recent inf-sup stable discretizations based on discontinuous multipliers such as  $\mathcal{Q}^2 - \mathcal{Q}^2 - \mathcal{Q}^0$  or  $\mathcal{Q}^1 - (\mathcal{Q}^1 + \mathfrak{B}) - \mathcal{Q}^0$  lead to  $\dim(V_{2,h}) \neq \dim(\Lambda_h)$ , and hence to a rectangular matrix  $\mathbf{C}_2$ . We stress, however, that the forthcoming spectral analysis will hold regardless of the specific choice of finite element spaces, as long as inf-sup stability is guaranteed.*

*For ease of implementation, we employ a square mass matrix in most of the numerical experiments. However, we also present results obtained using a discontinuous space for the multiplier. The influence of this choice on the performance of a multigrid preconditioner for this problem has been recently investigated in [2].*

We point out that the flexibility of employing independent meshes for  $\Omega$  and  $\Omega_2$  comes at the price of a certain implementation effort. The assembly procedure for the interface matrix  $\mathbf{C}$  is far from trivial. Indeed, the evaluation of  $c(\cdot, \cdot)$  as a standard  $L^2(\Omega_2)$  scalar product requires the integration of the product of two basis functions,  $\psi_k$  and  $\varphi_i$ , over the immersed mesh  $\mathcal{T}_{2,h}$ . However,  $\psi_k$  is defined on the mesh  $\mathcal{T}_{2,h}$ , while  $\varphi_i$  is defined on the background mesh  $\mathcal{T}_h$ . The efficient numerical integration of such terms requires the usage of suitable geometric search procedures and efficient collision detection algorithms, to identify pairs of background and immersed elements that overlap. The interested reader can find detailed discussions about this topic in [4, 20, 22, 23]. Finally, by virtue of the inf-sup condition in (13), matrix  $\mathbf{C}$  must have full row rank.

### 3. AUGMENTED LAGRANGIAN-BASED PRECONDITIONING

In this section, we derive an augmented Lagrangian-based preconditioner for the linear system (14), extending the strategy investigated in [11] for preconditioning other fictitious domain formulations. The derivation follows the AL approach introduced in [14] for the Oseen problem. The fundamental idea behind the AL approach is to replace the original linear system

$$(17) \quad \begin{bmatrix} \mathbf{A} & 0 & \mathbf{C}^\top \\ 0 & \mathbf{A}_2 & -\mathbf{C}_2^\top \\ \mathbf{C} & -\mathbf{C}_2 & 0 \end{bmatrix} \begin{bmatrix} \mathbf{u} \\ \mathbf{u}_2 \\ \lambda \end{bmatrix} = \begin{bmatrix} \mathbf{f} \\ \mathbf{g} \\ 0 \end{bmatrix} \quad \text{or} \quad \mathcal{A}\mathbf{x} = \mathbf{b},$$

with an equivalent formulation. To this end, let us introduce a strictly positive real number  $\gamma$ , and a symmetric and positive definite matrix  $W$  that will need to be chosen properly. Our goal is to exploit the constraint imposed by the last row of the system. To do so, we start by augmenting the first equation with the term  $\gamma C^T W^{-1} C u$ , obtaining

$$(18) \quad A u + C^T \lambda + \gamma C^T W^{-1} C u = f + \gamma C^T W^{-1} C u.$$

The last row of the system gives  $C u = C_2 u_2$ , which plugged into (18) gives

$$(19) \quad (A + \gamma C^T W^{-1} C) u - \gamma C^T W^{-1} C_2 u_2 + C^T \lambda = f.$$

Proceeding in the same vein, we augment the second row with the term  $\gamma C_2^T W^{-1} C_2 u_2$ , which yields

$$(20) \quad -\gamma C_2 W^{-1} C u + (A_2 + \gamma C_2^T W^{-1} C_2) u_2 - C_2 \lambda = g.$$

With Equations (18) and (20), the whole augmented system reads:

$$(21) \quad \begin{bmatrix} A + \gamma C^T W^{-1} C & -\gamma C^T W^{-1} C_2 & C^T \\ -\gamma C_2^T W^{-1} C & A_2 + \gamma C_2^T W^{-1} C_2 & -C_2^T \\ C & -C_2 & 0 \end{bmatrix} \begin{bmatrix} u \\ u_2 \\ \lambda \end{bmatrix} = \begin{bmatrix} f \\ g \\ 0 \end{bmatrix} \quad \text{or} \quad \mathcal{A}_\gamma x = b.$$

Having defined the augmented 2 by 2 block as:

$$(22) \quad \mathcal{A}_\gamma := \begin{bmatrix} A + \gamma C^T W^{-1} C & -\gamma C^T W^{-1} C_2 \\ -\gamma C_2^T W^{-1} C & A_2 + \gamma C_2^T W^{-1} C_2 \end{bmatrix},$$

and the operator pair  $B$  as

$$(23) \quad B := [C \quad -C_2],$$

we have that the system matrix in (21) can be rewritten (in compact form) as

$$(24) \quad \mathcal{A}_\gamma := \begin{bmatrix} \mathcal{A}_\gamma & B^T \\ B & 0 \end{bmatrix}.$$

Notably, the augmentation also removes the singularity in the original (2, 2)-block of the system (cf. Remark 1). Moreover,  $\mathcal{A}_\gamma$  can be expressed as:

$$(25) \quad \mathcal{A}_\gamma = \tilde{A} + \gamma B^T W^{-1} B,$$

where

$$(26) \quad \tilde{A} := \begin{bmatrix} A & 0 \\ 0 & A_2 \end{bmatrix}.$$

Therefore, since problem (17) has a unique solution and  $\tilde{A}$  is SPSD,  $\ker(\tilde{A}) \cap \ker(B) = \{0\}$ <sup>1</sup> and  $\mathcal{A}_\gamma$  is SPD [12]. An *ideal* [14] preconditioner for the augmented linear system is given by the block triangular matrix

$$(27) \quad \mathcal{P}_\gamma := \begin{bmatrix} \mathcal{A}_\gamma & B^T \\ 0 & -\frac{1}{\gamma} W \end{bmatrix}.$$

In practice, the action of  $\mathcal{P}_\gamma^{-1}$  is given by

$$\mathcal{P}_\gamma^{-1} = \begin{bmatrix} \mathcal{A}_\gamma^{-1} & 0 \\ 0 & I_\ell \end{bmatrix} \begin{bmatrix} I_{n+m} & B^T \\ 0 & -I_\ell \end{bmatrix} \begin{bmatrix} I_{n+m} & 0 \\ 0 & \gamma W^{-1} \end{bmatrix},$$

where  $I_{n+m}$  and  $I_\ell$  are identity matrices of size  $n+m$  and  $l$ , respectively. The last identity implies that the application of the preconditioner to a vector requires one solve with  $W$ , and one solve with the augmented term  $\mathcal{A}_\gamma$ . The solve with  $\mathcal{A}_\gamma$  does not need to be exact, and can be approximated by an inner iteration with a loose tolerance (e.g.,  $10^{-2}$ ), which is usually sufficient to keep the number of outer iterations

---

<sup>1</sup>This algebraic condition can be seen as an implicit consequence of the *discrete ellipticity on the kernel* condition stated in Proposition 2.

low when combined with (flexible) GMRES. Nevertheless, this step can still be challenging due to the large kernel of  $\mathbf{B}^\top \mathbf{W}^{-1} \mathbf{B}$ . In addition, increasing  $\gamma$  leads to a growth in the condition number of  $\mathbf{A}_\gamma$ , which may affect the convergence of iterative solvers. Strategies to overcome this issue are discussed in Section 5, where we consider some alternatives which can provide cheaper, inexact approximations. For now, we proceed with the *ideal* preconditioner in (27). The inner iteration for the augmented block must therefore be preconditioned; however, several preconditioning strategies rely on the explicit assembly of the augmented term  $\mathbf{A}_\gamma$ , leading to substantial memory and computational overhead, primarily due to the loss of sparsity.

Given the promising results obtained in [11] in the fictitious domain-type context,  $\mathbf{W}$  is chosen as

$$(28) \quad \mathbf{W} := \mathbf{M}^2,$$

where  $\mathbf{M}$  is the mass matrix on the multiplier space  $\Lambda$  defined in Equation (16). The reason for this choice will become clear in Section 4, where we perform a spectral analysis of the ideal preconditioner (27). Specifically, setting  $\mathbf{W} := \mathbf{M}^2$  ensures that the eigenvalues of the preconditioned matrix remain bounded away from zero uniformly in  $h_\Omega$ ,  $h_{\Omega_2}$  and, in practice, also fairly insensitive with respect to the jump in the coefficients  $\beta_2 - \beta$  (see Theorem 3).

In the particular case when  $V_{2,h} \equiv \Lambda_h$  (see Remark 2), one has  $\mathbf{C}_2 = \mathbf{M}$ . With this specific choice for  $\mathbf{W}$ , the (2, 2)-block reduces to the SPD matrix  $\mathbf{A}_2 + \gamma \mathbf{l}_m$ . This avoids potential loss of sparsity and allows the direct assembly of this augmented term, without the need to perform additional sparse matrix-matrix products.

**Remark 3** (Case  $V_{2,h} \neq \Lambda_h$ ). *In the general case  $V_{2,h} \neq \Lambda_h$ , the augmented diagonal (2, 2)-block  $\mathbf{A}_2 + \gamma \mathbf{C}_2^\top \mathbf{W}^{-1} \mathbf{C}_2$  is still positive definite even though it is a sum of two positive semi-definite matrices. This follows upon noticing that  $\ker(\mathbf{A}_2) = \text{span}\{\mathbf{1}\}$ , but  $\mathbf{1} \notin \ker(\mathbf{C}_2)^2$ . Hence,  $\ker(\mathbf{A}_2) \cap \ker(\mathbf{C}_2) = \{0\}$ , which implies the positive definiteness of the whole sum. This allows the spectral analysis performed in Section 6 to be general, and not tailored to a specific choice of the finite element discretization.*

#### 4. SPECTRAL ANALYSIS OF IDEAL PRECONDITIONER

In this Section, we derive lower and upper bounds for the eigenvalues of the preconditioned matrix  $\mathcal{P}_\gamma^{-1} \mathcal{A}_\gamma$ . Although eigenvalue information alone is generally insufficient to predict the convergence behavior of non-symmetric Krylov subspace methods [41], practical experience suggests that convergence is often fast when the spectrum is real, positive and confined within a moderately sized interval bounded away from 0. We will show that the eigenvalues of  $\mathcal{P}_\gamma^{-1} \mathcal{A}_\gamma$  cluster towards 1 as the augmentation parameter  $\gamma$  increases, confirming the usual behavior of AL-based preconditioners. Then, we will address mesh-independence of the smallest eigenvalue with respect to discretization parameters. We first recall the following result about generalized Rayleigh quotients.

**Lemma 1.** *Let  $\mathbf{Q}$  and  $\mathbf{N}$  be symmetric and symmetric positive definite matrices, respectively, with generalized eigenvalues  $\lambda_1 \leq \dots \leq \lambda_n$  and eigenvectors  $\mathbf{v}_1, \dots, \mathbf{v}_n \in \mathbb{R}^n$ , such that  $\mathbf{Q}\mathbf{v}_i = \lambda_i \mathbf{N}\mathbf{v}_i$ . Then:*

- *The smallest eigenvalue  $\lambda_1$  can be characterized as*

$$\lambda_1 = \min_{\mathbf{x} \neq 0} \frac{\mathbf{x}^\top \mathbf{Q} \mathbf{x}}{\mathbf{x}^\top \mathbf{N} \mathbf{x}}, \quad \text{achieved when } \mathbf{x} = \pm \mathbf{v}_1.$$

- *The second smallest eigenvalue  $\lambda_2$  satisfies*

$$\lambda_2 = \min_{\substack{\mathbf{x} \neq 0 \\ \mathbf{x}^\top \mathbf{N} \mathbf{v}_1 = 0}} \frac{\mathbf{x}^\top \mathbf{Q} \mathbf{x}}{\mathbf{x}^\top \mathbf{N} \mathbf{x}}, \quad \text{achieved when } \mathbf{x} = \pm \mathbf{v}_2,$$

and so on.

---

<sup>2</sup>This can be verified by explicit computation using the definition of  $\mathbf{C}_2$  in (15), together with the fact that  $\{\phi_j\}_{j=1}^m$  and  $\{\psi_j\}_{j=1}^m$  are basis sets.

**Theorem 1** (Spectrum of preconditioned matrix). *Assume that  $\mathcal{A}_\gamma$  and  $\mathcal{P}_\gamma$  are defined by the matrices in Equations (24) and (27), respectively. The eigenvalues of the preconditioned matrix  $\mathcal{P}_\gamma^{-1}\mathcal{A}_\gamma$  are all real and positive. More precisely, let  $\tilde{\mathbf{A}}$  be defined as in (26) and  $(\mathbf{x}; \mathbf{y})$  be an eigenvector of  $\mathcal{P}_\gamma^{-1}\mathcal{A}_\gamma$ . It holds*

$$\text{Spec}(\mathcal{P}_\gamma^{-1}\mathcal{A}_\gamma) \subseteq [\eta, 1],$$

where

$$\eta := \min_{\mathbf{x} \in \mathcal{S}} \frac{\gamma \mathbf{x}^\top \mathbf{B}^\top \mathbf{W}^{-1} \mathbf{B} \mathbf{x}}{\mathbf{x}^\top \tilde{\mathbf{A}} \mathbf{x} + \gamma \mathbf{x}^\top \mathbf{B}^\top \mathbf{W}^{-1} \mathbf{B} \mathbf{x}},$$

and with  $\lambda = 1$  being an eigenvalue of algebraic multiplicity at least  $n + m$ . Here  $\mathcal{S}$  denotes the set  $\mathcal{S} := \{\mathbf{v} \in \mathbb{R}^{n+m} \mid \mathbf{u}^\top \tilde{\mathbf{A}} \mathbf{v} = 0 \text{ for } \mathbf{u} \in \ker(\mathbf{B})\}$ .

*Proof.* Let  $\lambda \neq 0$  be an arbitrary eigenvalue of the preconditioned matrix, with a corresponding eigenvector  $(\mathbf{x}; \mathbf{y})$ . Since both the original system matrix (24) and the preconditioner (27) are nonsingular, the preconditioned matrix is also nonsingular, and therefore  $\lambda = 0$  cannot be an eigenvalue.

Notice that  $\mathbf{x}$  is actually a *block* vector, which means that  $\mathbf{x} = (\mathbf{x}_1; \mathbf{x}_2)$ , with  $\mathbf{x}_1 \in \mathbb{R}^n$  and  $\mathbf{x}_2 \in \mathbb{R}^m$ . The generalized eigenvalue problem can be stated as:

$$(29) \quad \begin{bmatrix} \mathbf{A}_\gamma & \mathbf{B}^\top \\ \mathbf{B} & 0 \end{bmatrix} \begin{bmatrix} \mathbf{x} \\ \mathbf{y} \end{bmatrix} = \lambda \begin{bmatrix} \mathbf{A}_\gamma & \mathbf{B}^\top \\ 0 & -\frac{1}{\gamma} \mathbf{W} \end{bmatrix} \begin{bmatrix} \mathbf{x} \\ \mathbf{y} \end{bmatrix},$$

which can be written explicitly as the following system of equations:

$$(30) \quad \mathbf{A}_\gamma \mathbf{x} + \mathbf{B}^\top \mathbf{y} = \lambda (\mathbf{A}_\gamma \mathbf{x} + \mathbf{B}^\top \mathbf{y}),$$

$$(31) \quad \mathbf{B} \mathbf{x} = -\frac{\lambda}{\gamma} \mathbf{W} \mathbf{y}.$$

Notice that  $\mathbf{x} \neq 0$ ; otherwise, the positive definiteness of  $\mathbf{W}$  implies  $\mathbf{y} = 0$ , in contradiction with the fact that  $(\mathbf{x}, \mathbf{y})$  is an eigenvector. Therefore, we can assume  $\mathbf{x} \neq 0$ .

It is evident from Equation (30) that  $\lambda = 1$  is an eigenvalue of  $\mathcal{P}_\gamma^{-1}\mathcal{A}_\gamma$ , with associated eigenvector  $(\mathbf{x}; -\gamma \mathbf{W}^{-1} \mathbf{B} \mathbf{x})$  when  $\mathbf{x} \notin \ker(\mathbf{B})$ . Moreover, when  $\mathbf{x} \in \ker(\mathbf{B})$ , we have  $(\mathbf{x}; 0)$  as associated eigenvector.

We now assume  $\lambda \neq 1$ . From (30) we derive

$$(32) \quad \mathbf{A}_\gamma \mathbf{x} + \mathbf{B}^\top \mathbf{y} = 0,$$

whereas from (31) we obtain  $\mathbf{y} = -\frac{\gamma}{\lambda} \mathbf{W}^{-1} \mathbf{B} \mathbf{x}$ , which plugged into the previous equation gives

$$(33) \quad \mathbf{A}_\gamma \mathbf{x} - \frac{\gamma}{\lambda} \mathbf{B}^\top \mathbf{W}^{-1} \mathbf{B} \mathbf{x} = 0.$$

Multiplying both sides of (33) by  $\lambda \mathbf{x}^*$ , we get

$$(34) \quad \lambda \mathbf{x}^* \mathbf{A}_\gamma \mathbf{x} - \gamma \mathbf{x}^* \mathbf{B}^\top \mathbf{W}^{-1} \mathbf{B} \mathbf{x} = 0,$$

and using (25), we obtain the following explicit equation for  $\lambda$

$$(35) \quad \lambda = \frac{\gamma \mathbf{x}^* \mathbf{B}^\top \mathbf{W}^{-1} \mathbf{B} \mathbf{x}}{\mathbf{x}^* \tilde{\mathbf{A}} \mathbf{x} + \gamma \mathbf{x}^* \mathbf{B}^\top \mathbf{W}^{-1} \mathbf{B} \mathbf{x}}.$$

The positive definiteness of  $\mathbf{A}_\gamma$  and the positive semidefiniteness of  $\mathbf{B}^\top \mathbf{W}^{-1} \mathbf{B}$  imply that all the eigenvalues are positive and real<sup>3</sup>. Moreover, note that in this case  $\mathbf{x}$  cannot belong to  $\ker(\tilde{\mathbf{A}})$ , since we are assuming  $\lambda \neq 1$ , nor to  $\ker(\mathbf{B})$  since  $\lambda \neq 0$ .

From (35) we also deduce that  $\lambda < 1$ , and that all eigenvalues satisfying (35) cluster towards 1 as  $\gamma \rightarrow +\infty$ , consistently with the theory of classical AL-based preconditioners [14]. We know that all nonunit eigenvalues of  $\mathcal{P}_\gamma^{-1}\mathcal{A}_\gamma$  satisfy (34), hence the smallest eigenvalue can be characterized using Lemma 1:

$$\eta := \min_{\mathbf{x} \in \mathcal{S}} \frac{\gamma \mathbf{x}^\top \mathbf{B}^\top \mathbf{W}^{-1} \mathbf{B} \mathbf{x}}{\mathbf{x}^\top \tilde{\mathbf{A}} \mathbf{x} + \gamma \mathbf{x}^\top \mathbf{B}^\top \mathbf{W}^{-1} \mathbf{B} \mathbf{x}},$$

<sup>3</sup>Hence, the corresponding eigenvector can also be chosen to be real: for this reason  $\mathbf{x}^*$  will be replaced by  $\mathbf{x}^\top$ .

which concludes the proof.  $\square$

**4.1. Numerical test: spectrum of preconditioned system.** We perform some preliminary numerical experiments to illustrate the impact of the preconditioner  $\mathcal{P}_\gamma$  on the spectrum of the original augmented system in (21). In particular, we examine how the distribution of the eigenvalues of the preconditioned matrix changes when varying  $\gamma$  and the magnitude of the coefficient jump  $\beta_2 - \beta$ . We will use  $\mathcal{Q}^1$  Lagrangian elements for all the finite element spaces involved in the formulation. We consider the following geometric configuration:

- $\Omega = [0, 1]^2$ ,
- $\Omega_2 = [0.2, 0.5]^2$ ,
- $\beta = 1$ ,

and a discretization for which  $A \in \mathbb{R}^{1089 \times 1089}$ ,  $A_2 \in \mathbb{R}^{81 \times 81}$ ,  $C_2 \in \mathbb{R}^{81 \times 81}$ , and  $C \in \mathbb{R}^{81 \times 1089}$ . The global system has then size 1251. Our choice for  $W$  is  $M^2$ . Eigenvalues have been computed using the `eig` function from MATLAB.

We report in Figure 2 the spectrum of the unpreconditioned matrix (top row, in magenta) and preconditioned matrix (bottom row, in green) for increasing values of the augmentation parameter  $\gamma$  and a fixed value  $\beta_2 = 100$ . We note that the system is not singular, but shows some small negative eigenvalues clustered near the origin, according to the indefinite nature of the saddle point system. Some observations can already be drawn from this Figure. First, the computed eigenvalues are all positive and real, thus confirming the first part of Theorem 1. As expected, higher values of the augmentation parameter  $\gamma$  result in a wider spectrum for the original system  $\mathcal{A}_\gamma$ . The bottom row shows the nice effect of the preconditioner  $\mathcal{P}_\gamma$ , which clusters the spectrum near one.

We perform the same test, setting this time  $\beta_2 = 10^6$ . The numerical findings are shown in Figure 3. We observe the spectrum of the original matrix to scale with the size of the jump. In contrast, the spectrum of the preconditioned matrix is essentially identical to the one in the bottom row of the previous figure, indicating that the preconditioner  $\mathcal{P}_\gamma$  remains quite effective in clustering the eigenvalues also for higher contrast in the coefficients.

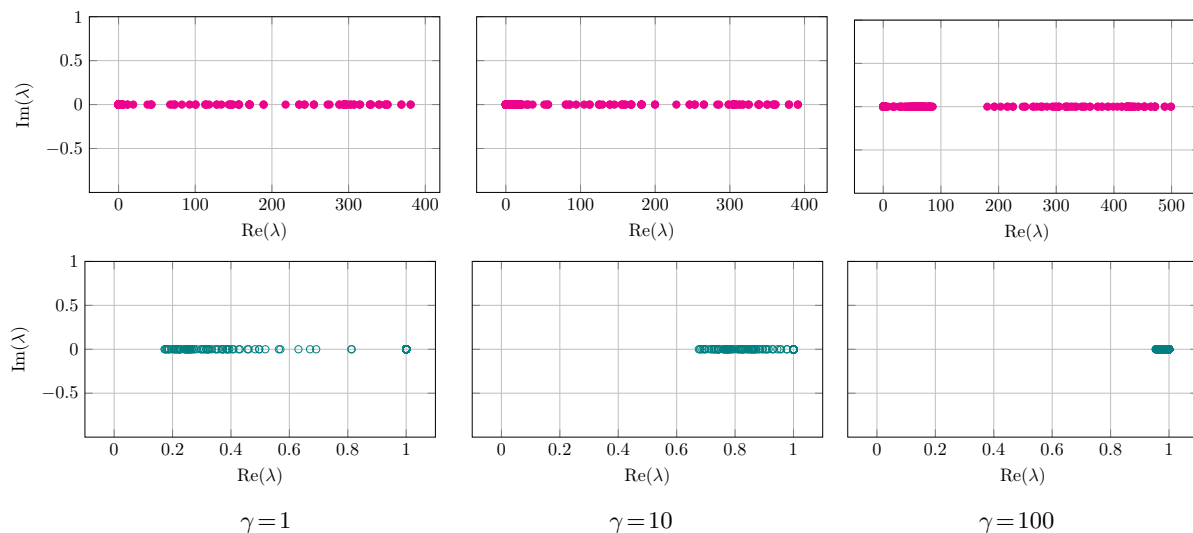


FIGURE 2.  $\beta = 1$ ,  $\beta_2 = 100$ . Spectrum of the original system matrix  $\mathcal{A}_\gamma$  (top row, in magenta) and  $\mathcal{P}_\gamma^{-1}\mathcal{A}_\gamma$  (bottom row, in green) for increasing values of the augmentation parameter  $\gamma$ .

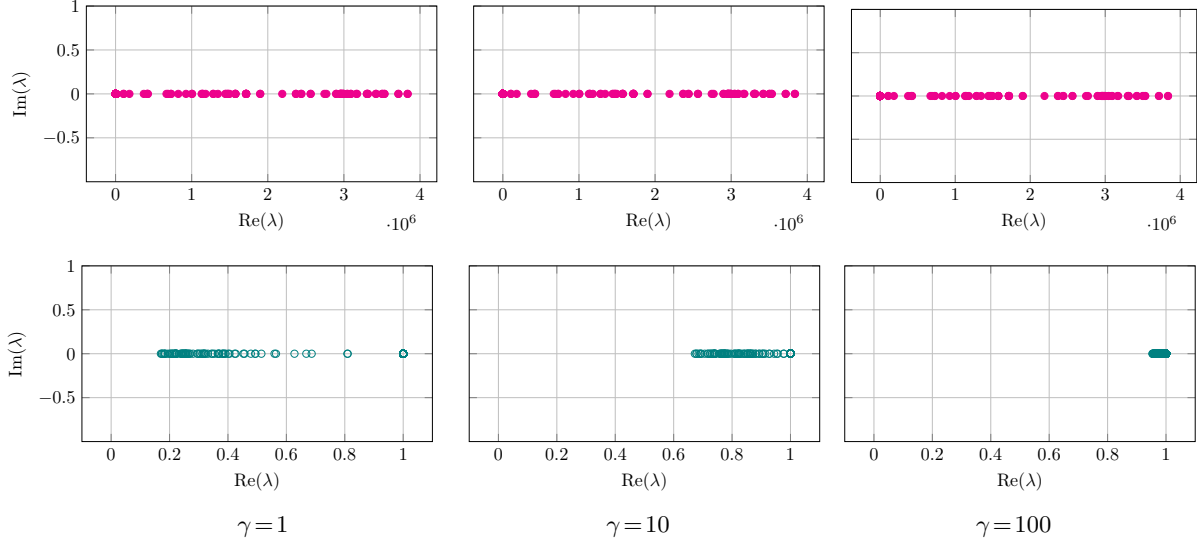


FIGURE 3.  $\beta = 1$ ,  $\beta_2 = 10^6$ . Spectrum of the original system matrix  $\mathcal{A}_\gamma$  (top row, in magenta) and  $\mathcal{P}_\gamma^{-1}\mathcal{A}_\gamma$  (bottom row, in green) for increasing values of the augmentation parameter  $\gamma$ . Notice the different scale in the x-axis of the first row.

**4.2. Mesh-independence of lower bound  $\eta$ .** Concerning the choice  $W = M^2$ , we will show that this selection is motivated by its property of ensuring that the lower bound  $\eta$  in Theorem 1 remains uniformly bounded away from zero with respect to mesh sizes  $h_\Omega$ ,  $h_{\Omega_2}$ , with dependence on the problem coefficients that will be made explicit. We stress that this only requires inf-sup stable spaces.

Before addressing the proof, we collect some useful technical results that will be used in the sequel.

**Lemma 2** (Spectral equivalence with  $h$ -scaled mass matrix). *Let  $d = 2$ ,  $M$  be the mass matrix defined on the multiplier space introduced in Section 2, and let  $h_{\Omega_2}$  denote the mesh size of  $\mathcal{T}_{2,h}$ . Then, the matrices  $h_{\Omega_2}^{-2}M^{-1}$  and  $M^{-2}$  are spectrally equivalent, i.e. there exist constants  $c_1, C_2$ , independent of the discretization parameters, such that*

$$(36) \quad 0 < c_1 \leq \frac{\mathbf{w}^\top M^{-2} \mathbf{w}}{\mathbf{w}^\top h_{\Omega_2}^{-2} M^{-1} \mathbf{w}} \leq C_2, \quad \forall \mathbf{w} \in \mathbb{R}^\ell, \mathbf{w} \neq 0.$$

*Considerations about the case  $d = 3$  will be discussed later.*

*Proof.* Let  $0 \neq \mathbf{w} \in \mathbb{R}^\ell$  be an arbitrary vector. Recall that two families of SPD matrices  $\{Q_\ell\}$  and  $\{N_\ell\}$  (parametrized by their dimension  $\ell$ ) are said to be *spectrally equivalent* if there exist  $\ell$ -independent constants  $c_1$  and  $C_2$  with

$$0 < c_1 \leq \frac{\mathbf{w}^\top Q_\ell \mathbf{w}}{\mathbf{w}^\top N_\ell \mathbf{w}} \leq C_2.$$

We drop the subscript  $\ell$ . We first multiply and then divide the generalized Rayleigh quotient in (36) by  $\mathbf{w}^\top \mathbf{w}$ , so that it can be rewritten in terms of the two Rayleigh quotients associated with the matrices  $(h_{\Omega_2}^2 M)^{-1}$  and  $M^{-2}$ .

For a general Hermitian matrix  $H$ , its Rayleigh quotient lies in the interval  $[\lambda_{\min}(H), \lambda_{\max}(H)]$ . Hence, we get

$$(37) \quad \frac{\lambda_{\min}(h_{\Omega_2}^2 M)}{\lambda_{\max}(M^2)} \leq \frac{\mathbf{w}^\top M^{-2} \mathbf{w}}{\mathbf{w}^\top \mathbf{w}} \frac{\mathbf{w}^\top \mathbf{w}}{\mathbf{w}^\top h_{\Omega_2}^{-2} M^{-1} \mathbf{w}} \leq \frac{\lambda_{\max}(h_{\Omega_2}^2 M)}{\lambda_{\min}(M^2)}.$$

Since the immersed mesh  $\mathcal{T}_{2,h}$  is assumed to be discretized in a quasi-uniform fashion, the following bound (see e.g. [36]) on the eigenvalues of the mass matrix holds

$$ch_{\Omega_2}^2 \leq \frac{\mathbf{w}^\top \mathbf{M} \mathbf{w}}{\mathbf{w}^\top \mathbf{w}} \leq Ch_{\Omega_2}^2 \quad \forall \mathbf{w} \in \mathbb{R}^\ell,$$

for some positive constants  $c$  and  $C$  independent of the discretization parameters. Using this in (37) and noting that  $\lambda(h_{\Omega_2}^2 \mathbf{M}) = h_{\Omega_2}^2 \lambda(\mathbf{M})$  and  $\lambda(\mathbf{M}^2) = (\lambda(\mathbf{M}))^2$  yields

$$0 < \frac{c}{C^2} \leq \frac{\mathbf{w}^\top \mathbf{M}^{-2} \mathbf{w}}{\mathbf{w}^\top h_{\Omega_2}^{-2} \mathbf{M}^{-1} \mathbf{w}} \leq \frac{C}{c^2}, \quad \forall \mathbf{w} \in \mathbb{R}^\ell,$$

which concludes the proof upon setting  $c_1 = \frac{c}{C^2}$  and  $C_2 = \frac{C}{c^2}$ .  $\square$

The following result is based on the more general framework presented in [51] for computing the eigenvalues and eigenvectors of Hermitian matrix pencils  $\mathbf{Q} - \lambda \mathbf{N}$ , where  $\mathbf{N}$  may be indefinite and even singular. For clarity of presentation, we state it in Theorem 2 in a simplified form, since in our problem we work exclusively with symmetric positive definite and symmetric positive semidefinite matrices.

We refer to  $\mathbf{Q} - \lambda \mathbf{N}$  as a *positive semidefinite symmetric pencil* if both  $\mathbf{Q}$  and  $\mathbf{N}$  are symmetric and there exists a real scalar  $\lambda_0$  such that  $\mathbf{Q} - \lambda_0 \mathbf{N}$  is positive semidefinite. Moreover,  $\mathbf{Q} - \lambda \mathbf{N}$  has  $r = \text{rank}(\mathbf{N})$  finite eigenvalues, all of which are real. In the algebraic theory it is customary to say that the remaining eigenvalues are *infinite* and their corresponding eigenvectors belong to the kernel of  $\mathbf{N}$ .

**Theorem 2.** *Let  $\mathbf{Q} - \lambda \mathbf{N}$  be a positive semidefinite symmetric pencil, with  $\mathbf{Q}, \mathbf{N} \in \mathbb{R}^{n \times n}$ . Let  $\lambda_i$  be the finite eigenvalues of  $\mathbf{Q} - \lambda \mathbf{N}$  arranged in the order  $\lambda_1 \leq \lambda_2 \leq \dots \leq \lambda_r$ . Then*

$$\lambda_i = \inf_{\substack{\mathcal{X} \\ \dim \mathcal{X} = i}} \sup_{\substack{\mathbf{x} \in \mathcal{X} \\ \mathbf{x}^\top \mathbf{N} \mathbf{x} \neq 0}} \frac{\mathbf{x}^\top \mathbf{Q} \mathbf{x}}{\mathbf{x}^\top \mathbf{N} \mathbf{x}},$$

where  $\mathcal{X}$  is a subspace of  $\mathbb{R}^n$ .

This theorem demonstrates that the presence of infinite eigenvalues does not affect the minimax formulas (see also [55]). Note that, when  $\mathbf{N}$  is also positive definite, the associated eigenvalue problem is equivalent to a standard symmetric eigenvalue problem, and therefore the Courant-Fischer minimax principles continue to hold.

Finally, we define the following norms:

$$(38) \quad |v_h|_{\mathbf{A}, \Omega} := (\mathbf{v}_1^\top \mathbf{A} \mathbf{v}_1)^{1/2},$$

$$(39) \quad |v_{2,h}|_{\mathbf{A}_2, \Omega_2} := (\mathbf{v}_2^\top \mathbf{A}_2 \mathbf{v}_2)^{1/2},$$

$$(40) \quad \|\mu_h\|_{0, \Omega_2} := (\boldsymbol{\mu}^\top \mathbf{M} \boldsymbol{\mu})^{1/2},$$

where  $\mathbf{v}_1$ ,  $\mathbf{v}_2$ , and  $\boldsymbol{\mu}$  are vectors of the coefficients associated with the basis sets  $\{\varphi_i\}_{i=1}^n$ ,  $\{\phi_j\}_{j=1}^m$ , and  $\{\psi_k\}_{k=1}^\ell$ . The matrices  $\mathbf{A}$ ,  $\mathbf{A}_2$ , and  $\mathbf{M}$  are defined in Section 2.3.

The following Lemma provides an algebraic interpretation of the discrete inf-sup stability conditions presented in Section 2, and is based on the seminal work by Malkus [53], which gives a specific link between the discrete inf-sup constant and the eigenvalues of a generalized eigenvalue problem. The next proof will follow similar arguments to the ones in [11, Lemma 3].

**Lemma 3** (Algebraic inf-sup condition). *Let  $\mathbf{A}, \mathbf{A}_2, \mathbf{B}$  and  $\mathbf{M}$  be the matrices defined in previous sections, and assume that the discrete inf-sup condition in Proposition 3 is satisfied. Moreover, let  $\tilde{\mathbf{A}}$  be defined as in (26), and  $\tilde{\mathbf{M}}_2 = \begin{bmatrix} 0 & 0 \\ 0 & \mathbf{M}_2 \end{bmatrix}$ , being  $\mathbf{M}_2$  the mass matrix defined on  $V_{2,h}$ . Then, there exists a positive constant  $\bar{\theta}$  independent of the mesh sizes  $h_\Omega$  and  $h_{\Omega_2}$  (but depending on coefficients  $\beta$  and  $\beta_2$ ) such that*

$$(41) \quad \bar{\theta}^2 \leq \min_{\mathcal{S} \setminus \ker(\tilde{\mathbf{A}})} \frac{\mathbf{v}^\top \mathbf{B}^\top \mathbf{M}^{-2} \mathbf{B} \mathbf{v}}{\mathbf{v}^\top \tilde{\mathbf{A}} \mathbf{v}},$$

where  $\mathcal{S} := \{\mathbf{v} \in \mathbb{R}^{n+m} \mid \mathbf{u}^\top \tilde{\mathbf{A}} \mathbf{v} = 0 \text{ for } \mathbf{u} \in \ker(\mathbf{B})\}$ .

*Proof.* We start by recalling the following inverse inequality, valid for all  $\mu_h \in \Lambda_h$ :

$$(42) \quad \|\mu_h\|_{-1, \Omega_2} \geq Ch_{\Omega_2} \|\mu_h\|_{0, \Omega_2},$$

with  $C$  a positive constant independent of  $h_{\Omega_2}$  [4]. By definition of the norms in (38) and (39), and assuming constant coefficients  $\beta_i$  in each subdomain, we have

$$\begin{aligned} |v_h|_{\mathbf{A}, \Omega} &= \beta^{\frac{1}{2}} |v_h|_{1, \Omega}, \\ |v_{2,h}|_{\mathbf{A}_2, \Omega_2} &= (\beta_2 - \beta)^{\frac{1}{2}} |v_h|_{1, \Omega_2}. \end{aligned}$$

It is straightforward to verify that the sum of norms appearing in the denominator of the inf-sup condition (13) satisfies the following inequality

$$\max\{\beta, \beta_2 - \beta, 1\} (|v_h|_{1, \Omega}^2 + \|v_{2,h}\|_{1, \Omega_2}^2) \geq (|v_h|_{\mathbf{A}, \Omega}^2 + |v_{2,h}|_{\mathbf{A}_2, \Omega_2}^2 + \|v_{2,h}\|_{0, \Omega_2}^2).$$

Combining the above inequality with (13) and (42), we obtain the following *rescaled* inf-sup condition:

$$(43) \quad \inf_{\mu_h \in \Lambda_h} \sup_{(v_h, v_{2,h}) \in V_h \times V_{2,h}} \frac{(\mu_h, v_h|_{\Omega_2} - v_{2,h})_{\Omega_2}}{(|v_h|_{\mathbf{A}, \Omega}^2 + |v_{2,h}|_{\mathbf{A}_2, \Omega_2}^2 + \|v_{2,h}\|_{0, \Omega_2}^2)^{\frac{1}{2}} h_{\Omega_2} \|\mu_h\|_{0, \Omega_2}} \geq \tilde{\theta}.$$

where  $\tilde{\theta} := \frac{C\theta}{\sqrt{\max\{\beta, \beta_2 - \beta, 1\}}}$ , independently of the mesh sizes.

It is easy to see that  $\mathbf{v}^T (\tilde{\mathbf{A}} + \tilde{\mathbf{M}}_2) \mathbf{v}$  realizes the sum of norms appearing in the denominator of (43). Using the fact that  $(\mu_h, v_h|_{\Omega_2} - v_{2,h})_{\Omega_2} = \mathbf{v}^T \mathbf{B}^T \boldsymbol{\mu}$ , the discrete inf-sup condition in (43) can be rewritten in the following algebraic form:

$$(44) \quad \inf_{\boldsymbol{\mu} \neq 0} \sup_{\mathbf{v} \neq 0} \frac{\mathbf{v}^T \mathbf{B}^T \boldsymbol{\mu}}{(\mathbf{v}^T (\tilde{\mathbf{A}} + \tilde{\mathbf{M}}_2) \mathbf{v})^{\frac{1}{2}} (\boldsymbol{\mu}^T h_{\Omega_2}^2 \mathbf{M} \boldsymbol{\mu})^{\frac{1}{2}}} \geq \tilde{\theta}.$$

Then, we argue as in [53, Th. 2], and let  $0 < \sigma_1 \leq \sigma_2 \leq \dots \leq \sigma_\ell$  be the  $\ell$  largest eigenvalues of the eigenproblem

$$(45) \quad (\mathbf{B}^T h_{\Omega_2}^{-2} \mathbf{M}^{-1} \mathbf{B}) \mathbf{v} = \sigma (\tilde{\mathbf{A}} + \tilde{\mathbf{M}}_2) \mathbf{v}.$$

The constant appearing in Equation (44) is given by the square root of  $\sigma_1$ , which is thus independent of the mesh size (the proof follows by using the same approach of [53], where the classical Stokes problem was considered). By considering the properties of the generalized Rayleigh quotient, the following characterization holds:

$$(46) \quad \tilde{\theta}^2 = \sigma_1 = \min_{\mathcal{R}} \frac{\mathbf{v}^T \mathbf{B}^T h_{\Omega_2}^{-2} \mathbf{M}^{-1} \mathbf{B} \mathbf{v}}{\mathbf{v}^T (\tilde{\mathbf{A}} + \tilde{\mathbf{M}}_2) \mathbf{v}},$$

where  $\mathcal{R} := \{\mathbf{v} \in \mathbb{R}^{n+m} \mid \mathbf{u}^T (\tilde{\mathbf{A}} + \tilde{\mathbf{M}}_2) \mathbf{v} = 0 \text{ for } \mathbf{u} \in \ker(\mathbf{B})\}$ .

Using now the spectral equivalence established in Lemma 2 between  $h_{\Omega_2}^{-2} \mathbf{M}^{-1}$  and  $\mathbf{M}^{-2}$ , we have for a  $\mathbf{w} \in \mathbb{R}^\ell$ :

$$(47) \quad \frac{c}{C^2} \leq \frac{\mathbf{w}^T \mathbf{M}^{-2} \mathbf{w}}{\mathbf{w}^T h_{\Omega_2}^{-2} \mathbf{M}^{-1} \mathbf{w}} \leq \frac{C}{c^2},$$

where the positive constants  $c, C$  are independent of the discretization parameters. Setting  $\mathbf{w} = \mathbf{B} \mathbf{v}$ , and multiplying each term of (47) by  $\frac{\mathbf{w}^T (h_{\Omega_2}^2 \mathbf{M})^{-1} \mathbf{w}}{\mathbf{v}^T (\tilde{\mathbf{A}} + \tilde{\mathbf{M}}_2) \mathbf{v}}$ , we get

$$0 < \frac{c}{C^2} \frac{\mathbf{v}^T \mathbf{B}^T (h_{\Omega_2}^2 \mathbf{M})^{-1} \mathbf{B} \mathbf{v}}{\mathbf{v}^T (\tilde{\mathbf{A}} + \tilde{\mathbf{M}}_2) \mathbf{v}} \leq \frac{\mathbf{v}^T \mathbf{B}^T \mathbf{M}^{-2} \mathbf{B} \mathbf{v}}{\mathbf{v}^T (\tilde{\mathbf{A}} + \tilde{\mathbf{M}}_2) \mathbf{v}} \leq \frac{C}{c^2} \frac{\mathbf{v}^T \mathbf{B}^T (h_{\Omega_2}^2 \mathbf{M})^{-1} \mathbf{B} \mathbf{v}}{\mathbf{v}^T (\tilde{\mathbf{A}} + \tilde{\mathbf{M}}_2) \mathbf{v}}.$$

Combining this result with (46), it follows that

$$(48) \quad \bar{\theta}^2 \leq \min_{\mathcal{R}} \frac{\mathbf{v}^T \mathbf{B}^T \mathbf{M}^{-2} \mathbf{B} \mathbf{v}}{\mathbf{v}^T (\tilde{\mathbf{A}} + \tilde{\mathbf{M}}_2) \mathbf{v}},$$

(where  $\bar{\theta}^2 := \frac{c}{C^2} \sigma_1$ ), uniformly in  $h_\Omega$  and  $h_{\Omega_2}$ .

We now conclude the proof by comparing the generalized Rayleigh quotient in (48) with the one whose denominator is  $\mathbf{v}^\top \tilde{\mathbf{A}} \mathbf{v}$ . According to the theory of generalized eigenvalue problems [51], since  $\dim(\ker(\tilde{\mathbf{A}})) = 1$ , the matrix pencil  $\mathbf{B}^\top \mathbf{M}^{-2} \mathbf{B} - \lambda \tilde{\mathbf{A}}$  has exactly one infinite eigenvalue with eigenvector belonging to  $\ker(\tilde{\mathbf{A}})$ .

We have

$$(49) \quad \frac{\mathbf{v}^\top \mathbf{B}^\top \mathbf{M}^{-2} \mathbf{B} \mathbf{v}}{\mathbf{v}^\top (\tilde{\mathbf{A}} + \tilde{\mathbf{M}}_2) \mathbf{v}} \leq \frac{\mathbf{v}^\top \mathbf{B}^\top \mathbf{M}^{-2} \mathbf{B} \mathbf{v}}{\mathbf{v}^\top \tilde{\mathbf{A}} \mathbf{v}} \quad \forall \mathbf{v} \in \mathbb{R}^{n+m}, \text{ with } \mathbf{v} \notin \ker(\tilde{\mathbf{A}}).$$

Using this inequality together with Theorem 2, we can compare the eigenvalues of the two associated generalized eigenvalue problems. We note that the minimax characterization in Theorem 2 can naturally accommodate infinite eigenvalues. In particular, vectors in  $\ker(\tilde{\mathbf{A}})$  formally correspond to an infinite generalized eigenvalue in the second quotient, leaving the inequality trivially satisfied. In other words, in the right-hand side of the inequality above, including or excluding  $\ker(\tilde{\mathbf{A}})$  from the subspaces over which the minimax principle is taken, does not affect the smallest finite eigenvalue. Consequently, the restriction  $\mathbf{v}^\top \tilde{\mathbf{A}} \mathbf{v} \neq 0$  in the supremum can be removed, and we get:

$$\sigma_i \leq \inf_{\substack{\mathcal{X} \\ \dim \mathcal{X} = i}} \sup_{\mathbf{v} \in \mathcal{X}} \frac{\mathbf{v}^\top \mathbf{B}^\top \mathbf{M}^{-2} \mathbf{B} \mathbf{v}}{\mathbf{v}^\top (\tilde{\mathbf{A}} + \tilde{\mathbf{M}}_2) \mathbf{v}} \leq \inf_{\substack{\mathcal{X} \\ \dim \mathcal{X} = i}} \sup_{\mathbf{v} \in \mathcal{X}} \frac{\mathbf{v}^\top \mathbf{B}^\top \mathbf{M}^{-2} \mathbf{B} \mathbf{v}}{\mathbf{v}^\top \tilde{\mathbf{A}} \mathbf{v}} = \lambda_i,$$

where  $\sigma_i$  are the generalized eigenvalues of (45), while  $\lambda_i$  are those of  $\mathbf{B}^\top \mathbf{M}^{-2} \mathbf{B} \mathbf{v} = \lambda \tilde{\mathbf{A}} \mathbf{v}$ . Therefore, each  $\lambda_i$  is greater than or equal to the corresponding  $\sigma_i$ . This also applies to the smallest positive eigenvalue, and we obtain

$$\bar{\theta}^2 \leq \min_{\mathcal{S}} \frac{\mathbf{v}^\top \mathbf{B}^\top \mathbf{M}^{-2} \mathbf{B} \mathbf{v}}{\mathbf{v}^\top (\tilde{\mathbf{A}} + \tilde{\mathbf{M}}_2) \mathbf{v}} \leq \min_{\mathcal{S}} \frac{\mathbf{v}^\top \mathbf{B}^\top \mathbf{M}^{-2} \mathbf{B} \mathbf{v}}{\mathbf{v}^\top \tilde{\mathbf{A}} \mathbf{v}},$$

where  $\mathcal{S} := \{\mathbf{v} \in \mathbb{R}^{n+m} \mid \mathbf{u}^\top \tilde{\mathbf{A}} \mathbf{v} = 0 \text{ for } \mathbf{u} \in \ker(\mathbf{B})\}$ . The thesis follows from the observation that the minimization over  $\mathcal{S}$  is unaffected by the presence of  $\ker(\tilde{\mathbf{A}})$ . Therefore, minimizing over  $\mathcal{S}$  or over  $\mathcal{S} \setminus \ker(\tilde{\mathbf{A}})$  yields the same value.  $\square$

**Theorem 3** (Mesh-independence for lower bound). *Let  $V_h$ ,  $V_{2,h}$  and  $\Lambda_h$  be defined as in Section 2. If  $\mathbf{W} := \mathbf{M}^2$ , then the lower bound in*

$$\text{Spec}(\mathcal{P}_\gamma^{-1} \mathcal{A}_\gamma) \subseteq [\eta, 1]$$

*from Theorem 1 is bounded away from zero independently of the discretization parameters,  $h_\Omega$  and  $h_{\Omega_2}$  (but depending on coefficients  $\beta$  and  $\beta_2$ ).*

*Proof.* From the proof of Theorem 1 (more precisely from Equation (33)), we know that all nonunit eigenvalues of  $\mathcal{P}_\gamma^{-1} \mathcal{A}_\gamma$  coincide with the eigenvalues of the following generalized eigenvalue problem:

$$(50) \quad \gamma \mathbf{B}^\top \mathbf{W}^{-1} \mathbf{B} \mathbf{x} = \lambda (\tilde{\mathbf{A}} + \gamma \mathbf{B}^\top \mathbf{W}^{-1} \mathbf{B}) \mathbf{x},$$

excluding the cases  $\lambda = 0$  and  $\lambda = 1$ , which correspond respectively to eigenvectors  $\mathbf{x} \in \ker(\mathbf{B})$  and  $\mathbf{x} \in \ker(\tilde{\mathbf{A}})$ . Our goal is to show that  $\eta = \lambda_{\min}^+$ , the smallest positive eigenvalue of (50), is bounded away from zero. By Remark 1, this eigenvalue admits the Rayleigh quotient characterization

$$(51) \quad \eta = \min_{\mathbf{v} \in \mathcal{S}} \frac{\gamma \mathbf{v}^\top \mathbf{B}^\top \mathbf{W}^{-1} \mathbf{B} \mathbf{v}}{\mathbf{v}^\top (\tilde{\mathbf{A}} + \gamma \mathbf{B}^\top \mathbf{W}^{-1} \mathbf{B}) \mathbf{v}},$$

where  $\mathcal{S}$  is defined as

$$\mathcal{S} := \{\mathbf{v} \in \mathbb{R}^{n+m} : \mathbf{u}^\top (\tilde{\mathbf{A}} + \gamma \mathbf{B}^\top \mathbf{W}^{-1} \mathbf{B}) \mathbf{v} = 0 \quad \forall \mathbf{u} \in \ker(\mathbf{B})\}.$$

The condition  $\mathbf{u} \in \ker(\mathbf{B})$  gives the following alternative characterization of  $\mathcal{S}$ :

$$\mathcal{S} = \{\mathbf{v} \in \mathbb{R}^{n+m} : \mathbf{u}^\top \tilde{\mathbf{A}} \mathbf{v} = 0 \quad \forall \mathbf{u} \in \ker(\mathbf{B})\}.$$

Note that  $\mathcal{S}$  contains any nonzero vector in  $\ker(\tilde{\mathbf{A}})$ . However, such vectors correspond to the eigenvalue  $\lambda = 1$  in (50), that is the largest eigenvalue rather than the smallest positive one. Nevertheless, it is convenient to exclude  $\ker(\tilde{\mathbf{A}})$  from  $\mathcal{S}$ , because for every  $\mathbf{v} \in \mathcal{S} \setminus \ker(\tilde{\mathbf{A}})$  we have  $\mathbf{v}^\top \tilde{\mathbf{A}} \mathbf{v} > 0$ , thus preventing

division by zero in the Rayleigh quotient below. This exclusion does not alter the value of the smallest finite eigenvalue, since minimizing over  $\mathcal{S}$  or over  $\mathcal{S} \setminus \ker(\tilde{\mathbf{A}})$  yields the same result for  $\eta$ .

Consequently, we may safely multiply and divide the Rayleigh quotient in (51) by  $\mathbf{v}^\top \tilde{\mathbf{A}} \mathbf{v}$ , and obtain

$$\eta = \min_{\mathbf{v} \in \mathcal{S} \setminus \ker(\tilde{\mathbf{A}})} \frac{\gamma \mathbf{v}^\top \mathbf{B}^\top \mathbf{W}^{-1} \mathbf{B} \mathbf{v}}{\mathbf{v}^\top \tilde{\mathbf{A}} \mathbf{v}} \frac{\mathbf{v}^\top \tilde{\mathbf{A}} \mathbf{v}}{\mathbf{v}^\top (\tilde{\mathbf{A}} + \gamma \mathbf{B}^\top \mathbf{W}^{-1} \mathbf{B}) \mathbf{v}}.$$

As long as the denominator is nonzero, we can define  $r(\mathbf{v}) := \frac{\mathbf{v}^\top \mathbf{B}^\top \mathbf{W}^{-1} \mathbf{B} \mathbf{v}}{\mathbf{v}^\top \tilde{\mathbf{A}} \mathbf{v}}$  as the generalized Rayleigh quotient associated with  $\mathbf{B}^\top \mathbf{W}^{-1} \mathbf{B}$  and  $\tilde{\mathbf{A}}$ . We observe that  $\eta$  can be written as

$$\eta = \min_{\mathbf{v} \in \mathcal{S} \setminus \ker(\tilde{\mathbf{A}})} \frac{\gamma r(\mathbf{v})}{1 + \gamma r(\mathbf{v})} = \min_{\mathbf{v} \in \mathcal{S} \setminus \ker(\tilde{\mathbf{A}})} f(r(\mathbf{v})).$$

Since  $f_\gamma : x \mapsto \frac{\gamma x}{1 + \gamma x}$  is a monotone increasing function for  $x > 0$ ,

$$\min_{\mathbf{v} \in \mathcal{S} \setminus \ker(\tilde{\mathbf{A}})} f(r(\mathbf{v})) = f\left(\min_{\mathbf{v} \in \mathcal{S} \setminus \ker(\tilde{\mathbf{A}})} r(\mathbf{v})\right).$$

Choosing  $\mathbf{W} = \mathbf{M}^2$ , from Lemma 3 we conclude that

$$(52) \quad \eta \geq f(\bar{\theta}^2) = \frac{\gamma \bar{\theta}^2}{1 + \gamma \bar{\theta}^2} > 0.$$

□

**Remark 4** (Three-dimensional case). *When  $d = 3$ , using the same arguments as above, we get*

$$\eta \geq f(\bar{\theta}^2) = \frac{\gamma \bar{\theta}^2}{h_{\Omega_2} + \gamma \bar{\theta}^2} > 0.$$

*To show this, assuming a quasi-uniform discretization for  $\mathcal{T}_{2,h}$ , it holds:*

$$(53) \quad ch_{\Omega_2}^3 \leq \frac{\mathbf{w}^\top \mathbf{M} \mathbf{w}}{\mathbf{w}^\top \mathbf{w}} \leq Ch_{\Omega_2}^3 \quad \forall \mathbf{w} \in \mathbb{R}^\ell,$$

*yielding*

$$(54) \quad 0 < \frac{c}{C^2 h_{\Omega_2}} \leq \frac{\mathbf{w}^\top \mathbf{M}^{-2} \mathbf{w}}{\mathbf{w}^\top (h_{\Omega_2}^2 \mathbf{M})^{-1} \mathbf{w}} \leq \frac{C}{c^2 h_{\Omega_2}}.$$

*Setting again  $\mathbf{w} = \mathbf{B} \mathbf{v}$  in the proof of Lemma 3, it holds that*

$$(55) \quad \min_{\{\mathbf{v} \in \mathbb{R}^{n+m} \mid \mathbf{u}^\top \tilde{\mathbf{A}} \mathbf{v} = 0 \text{ for } \mathbf{u} \in \ker(\mathbf{B})\}} \frac{\mathbf{v}^\top \mathbf{B}^\top \mathbf{M}^{-2} \mathbf{B} \mathbf{v}}{\mathbf{v}^\top \tilde{\mathbf{A}} \mathbf{v}} \geq \frac{c}{C^2} \frac{\tilde{\theta}^2}{h_{\Omega_2}}.$$

*Following the same steps used to derive Equation (52), we employ the inequality in (55) above to obtain*

$$(56) \quad 0 < \frac{\gamma \tilde{\theta}^2}{h_{\Omega_2} + \gamma \tilde{\theta}^2} \lesssim \eta.$$

*Notice how in this case the lower bound for the eigenvalues of the preconditioned matrix depends explicitly on  $h_{\Omega_2}$ . However, it is immediate to observe that as  $h_{\Omega_2} \rightarrow 0$ , the lower bound in (56) tends to 1. Therefore, we conclude that also in this scenario the bound is robust with respect to the discretization parameters.*

**Remark 5** (Parameter robustness). *From the previous proof and from Lemma 3, it follows that the lower bound obtained in Theorem 1 will in general depend on  $\beta$  and on the jump  $\beta_2 - \beta$  through the quantity  $\max\{\beta, \beta_2 - \beta, 1\}$ . In particular, these results show that choosing  $\gamma = \mathcal{O}(\max\{\beta, \beta_2 - \beta, 1\}^{-1})$  in (52) or (56) is sufficient to guarantee that all nonunit eigenvalues of  $\mathcal{P}_\gamma^{-1} \mathcal{A}_\gamma$  remain uniformly bounded away from 0. This behaviour is consistent with the observations reported in [14] for the Oseen problem, where the authors show that the spectral bounds of the preconditioned system depend on the viscosity  $\nu$ , and therefore a parameter choice of the form  $\gamma = \mathcal{O}(\nu^{-1})$  is theoretically required. As pointed out in [14], this theoretical guideline is of limited practical relevance. Indeed, in the numerical results in Section 7 we will observe that using a fixed value of  $\gamma$  already yields convergence of the Krylov subspace method*

that is independent of  $h_\Omega$ ,  $h_{\Omega_2}$ , the coefficients  $\beta$ ,  $\beta_2$ , and their jump  $\beta_2 - \beta$ , without the need to scale  $\gamma$  according to the problem parameters.

## 5. MODIFIED AL PRECONDITIONER

As shown in prior studies, e.g. [14, 16], the performance of the AL approach crucially depends on the availability of an effective approximate solver for the augmented block. However, as previously mentioned, developing such a solver is a nontrivial task. The main difficulty comes from the fact that when  $\gamma$  is large the augmented block becomes increasingly ill-conditioned. For this reason, in [14], a robust multigrid solver for it was proposed for the Oseen problem and later extended in [37] to the 3D case. We note that developing such a tailored solver in our setting is more cumbersome, due to the independence of the two grids  $\mathcal{T}_h$  and  $\mathcal{T}_{2,h}$ , which further complicates the development of possible multilevel approaches. Therefore, we adopt the modified AL approach proposed in [16], adjusted to take advantage of the specific properties of the elliptic interface problem.

In what follows, we recall the idea behind the modified AL approach, briefly referring to the context in which it was first introduced in [16], namely the Oseen problem. In this section,  $\mathbf{u}$  and  $\mathbf{p}$  denote nodal values for velocity and pressure, respectively, while  $\mathbf{N}$  and  $\mathbf{B}$  represent the discretizations of the diffusion–convection terms and (negative) divergence operator, respectively.

**5.1. Modified AL preconditioner for the Oseen problem.** Discretization of the Oseen equations using stable finite element pairs yields large, sparse linear systems of the form

$$(57) \quad \begin{bmatrix} \mathbf{N} & \mathbf{B}^\top \\ \mathbf{B} & \mathbf{0} \end{bmatrix} \begin{bmatrix} \mathbf{u} \\ \mathbf{p} \end{bmatrix} = \begin{bmatrix} \mathbf{f} \\ \mathbf{g} \end{bmatrix}.$$

The key observation is that, in two dimensions, the matrix  $\mathbf{N}$  associated with the convection-diffusion operator is block diagonal:  $\mathbf{N} = \text{diag}(\mathbf{N}_1, \mathbf{N}_2)$ , and writing  $\mathbf{B} = [\mathbf{B}_1 \quad \mathbf{B}_2]$ , the saddle-point matrix in (57) can be rewritten as

$$(58) \quad \mathcal{A} = \begin{bmatrix} \mathbf{N}_1 & \mathbf{0} & \mathbf{B}_1^\top \\ \mathbf{0} & \mathbf{N}_2 & \mathbf{B}_2^\top \\ \mathbf{B}_1 & \mathbf{B}_2 & \mathbf{0} \end{bmatrix}.$$

Therefore, the augmented (1, 1)-block can be written as

$$\mathbf{N}_\gamma = \mathbf{N} + \gamma \mathbf{B}^\top \mathbf{W}^{-1} \mathbf{B} = \begin{bmatrix} \mathbf{N}_1 + \gamma \mathbf{B}_1^\top \mathbf{W}^{-1} \mathbf{B}_1 & \gamma \mathbf{B}_1^\top \mathbf{W}^{-1} \mathbf{B}_2 \\ \gamma \mathbf{B}_2^\top \mathbf{W}^{-1} \mathbf{B}_1 & \mathbf{N}_2 + \gamma \mathbf{B}_2^\top \mathbf{W}^{-1} \mathbf{B}_2 \end{bmatrix} = \begin{bmatrix} \mathbf{N}_{11} & \mathbf{N}_{12} \\ \mathbf{N}_{21} & \mathbf{N}_{22} \end{bmatrix},$$

where  $\gamma$  is a positive scalar and  $\mathbf{W}$  is again a suitable SPD matrix. The *modified AL preconditioner* is then defined as the following block-triangular matrix:

$$\tilde{\mathcal{P}}_\gamma = \begin{bmatrix} \mathbf{N}_{11} & \mathbf{N}_{12} & \mathbf{B}_1^\top \\ \mathbf{0} & \mathbf{N}_{22} & \mathbf{B}_2^\top \\ \mathbf{0} & \mathbf{0} & \hat{\mathbf{S}} \end{bmatrix},$$

where  $\hat{\mathbf{S}}$  is taken as  $-\frac{1}{\gamma} \mathbf{M}_p$ , being  $\mathbf{M}_p$  the classical pressure mass matrix [17]. Due to the new block-triangular structure of  $\tilde{\mathcal{P}}_\gamma$ , most of the computational effort involved in applying  $\tilde{\mathcal{P}}_\gamma^{-1}$  to a vector reduces to solving two linear systems with matrices  $\mathbf{N}_{11}$  and  $\mathbf{N}_{22}$ . These two subsystems can be solved either exactly or approximately by means of iterative methods. The extension of this approach to 3D problems is immediate.

As pointed out in [16], the fact that the modified AL preconditioner is derived from the ideal one by neglecting a block of the form  $\gamma \mathbf{B}_2^\top \mathbf{W}^{-1} \mathbf{B}_1$  suggests that the parameter  $\gamma$  should not be chosen excessively large. Although the preconditioner is robust with respect to mesh refinement (see, e.g., the analysis in [15]), it still exhibits some dependence on the viscosity parameter.

**5.2. Modified AL preconditioner for elliptic interface problem.** Having introduced the idea behind the modified AL approach, we observe that the matrix  $\mathcal{A}$  in (58) shares the same *block structure* as our system matrix in (14). Hence, the natural structure of the preconditioner looks as follows:

$$(59) \quad \tilde{\mathcal{P}}_\gamma = \begin{bmatrix} A + \gamma C^T W^{-1} C & -\gamma C^T W^{-1} C_2 & C^T \\ 0 & A_2 + \gamma C_2^T W^{-1} C_2 & -C_2^T \\ 0 & 0 & \hat{S} \end{bmatrix}.$$

We note that, in our problem, the matrices  $A$  and  $A_2$  correspond to two *different* equations and are not associated with a block partitioning of unknowns for a single discrete operator, as was the case in the Oseen problem. The same applies to  $C$  and  $C_2$ , which in our problem denote two completely different operators, rather than two blocks of the same discrete operator in each coordinate direction, as  $B_1$  and  $B_2$ . This allows us to consider a different way of augmenting them. That is, we augment the first and second rows of the system with positive but different parameters  $\gamma_1$  and  $\gamma_2$ , respectively. This yields the following augmented system:

$$(60) \quad \begin{bmatrix} A + \gamma_1 C^T W^{-1} C & -\gamma_1 C^T W^{-1} C_2 & C^T \\ -\gamma_2 C_2^T W^{-1} C & A_2 + \gamma_2 C_2^T W^{-1} C_2 & -C_2^T \\ C & -C_2 & 0 \end{bmatrix} \begin{bmatrix} u \\ u_2 \\ \lambda \end{bmatrix} = \begin{bmatrix} f \\ g \\ 0 \end{bmatrix},$$

for which we propose the following *modified* AL preconditioner:

$$(61) \quad \tilde{\mathcal{P}}_{\gamma_1, \gamma_2} := \begin{bmatrix} A + \gamma_1 C^T W^{-1} C & -\gamma_1 C^T W^{-1} C_2 & C^T \\ 0 & A_2 + \gamma_2 C_2^T W^{-1} C_2 & -C_2^T \\ 0 & 0 & \hat{S} \end{bmatrix}.$$

The selection of  $\hat{S}$  will be detailed in the spectral analysis presented in Section 6, where we demonstrate that an appropriate choice is  $\hat{S} = -\frac{1}{\gamma_1} W$ . Note that the (2, 2)-block in (59) and (61) is nonsingular, owing to the fact that  $A_2$  is positive definite on  $\ker(C_2)$  (cf. Remark 1).

The main benefit of this new variant is that we can now select *different* values for the augmentation parameters  $\gamma_1$  and  $\gamma_2$ . In particular,  $\gamma_1$  can be taken large to ensure strong clustering of the eigenvalues, while  $\gamma_2$  can remain small, thereby mitigating the effect of dropping the (2, 1)-block. However, note that just as  $\gamma_1$  cannot be made too large, since this would render the augmented (1, 1)-block in (61) increasingly ill-conditioned,  $\gamma_2$  likewise cannot be taken too small, as this would make the augmented (2, 2)-block nearly singular, due to the semidefiniteness of  $A_2$ . We will see in the numerical experiments that, in contrast with classical modified approaches (such as in [16, 17]), we do not need to tune these parameters upon mesh refinement.

## 6. SPECTRAL ANALYSIS FOR THE MODIFIED PRECONDITIONER

In this section, we perform a spectral analysis for the modified AL preconditioner introduced in (61). Our derivation closely follows the spectral analysis developed in [17] for the modified AL preconditioner applied to the steady-state Navier-Stokes equations. We start by recalling the AL formulation (60):

$$(62) \quad \mathcal{A}_{\gamma_1, \gamma_2} := \begin{bmatrix} A + \gamma_1 C^T W^{-1} C & -\gamma_1 C^T W^{-1} C_2 & C^T \\ -\gamma_2 C_2^T W^{-1} C & A_2 + \gamma_2 C_2^T W^{-1} C_2 & -C_2^T \\ C & -C_2 & 0 \end{bmatrix} = \begin{bmatrix} A_{11} & A_{12} & C^T \\ A_{21} & A_{22} & -C_2^T \\ C & -C_2 & 0 \end{bmatrix},$$

and the associated modified AL preconditioner (61) when different parameters  $\gamma_1$  and  $\gamma_2$  are used:

$$(63) \quad \tilde{\mathcal{P}}_{\gamma_1, \gamma_2} = \begin{bmatrix} A_{11} & A_{12} & C^T \\ 0 & A_{22} & -C_2^T \\ 0 & 0 & \hat{S} \end{bmatrix} = \begin{bmatrix} \tilde{A}_{\gamma_1, \gamma_2}^{-1} & B^T \\ 0 & \hat{S} \end{bmatrix}.$$

The block upper-triangular structure of  $\tilde{\mathcal{P}}_{\gamma_1, \gamma_2}$  yields the following factorization:

$$(64) \quad \tilde{\mathcal{P}}_{\gamma_1, \gamma_2} = \begin{bmatrix} \tilde{\mathbf{A}}_{\gamma_1, \gamma_2}^{-1} & 0 \\ 0 & \mathbf{I}_\ell \end{bmatrix} \begin{bmatrix} \mathbf{I}_{n+m} & \mathbf{B}^\top \\ 0 & -\mathbf{I}_\ell \end{bmatrix} \begin{bmatrix} \mathbf{I}_{n+m} & 0 \\ 0 & -\hat{\mathbf{S}}^{-1} \end{bmatrix},$$

where

$$\tilde{\mathbf{A}}_{\gamma_1, \gamma_2} := \begin{bmatrix} \mathbf{A} + \gamma_1 \mathbf{C}^\top \mathbf{W}^{-1} \mathbf{C} & -\gamma_1 \mathbf{C}^\top \mathbf{W}^{-1} \mathbf{C}_2 \\ 0 & \mathbf{A}_2 + \gamma_2 \mathbf{C}_2^\top \mathbf{W}^{-1} \mathbf{C}_2 \end{bmatrix}.$$

The result stated in the lemma below is proved in Appendix A. Notice that all the necessary matrices are invertible (cf. Remark 3).

**Lemma 4.** *The right-preconditioned matrix has the following block structure:*

$$(65) \quad \mathcal{A}_{\gamma_1, \gamma_2} \tilde{\mathcal{P}}_{\gamma_1, \gamma_2}^{-1} = \begin{bmatrix} \mathbf{I}_n & 0 & 0 \\ \mathbf{A}_{21} \mathbf{A}_{11}^{-1} & \mathbf{I}_m - \mathbf{A}_{21} \mathbf{A}_{11}^{-1} \mathbf{A}_{12} \mathbf{A}_{22}^{-1} & \mathbf{T}_{23} \\ \mathbf{C} \mathbf{A}_{11}^{-1} & -\mathbf{C} \mathbf{A}_{11}^{-1} \mathbf{A}_{12} \mathbf{A}_{22}^{-1} - \mathbf{C}_2 \mathbf{A}_{22}^{-1} & \mathbf{T}_{33} \end{bmatrix}$$

where

$$\mathbf{T}_{23} = (-\mathbf{A}_{21} \mathbf{A}_{11}^{-1} \mathbf{C}^\top - \mathbf{A}_{21} \mathbf{A}_{11}^{-1} \mathbf{A}_{12} \mathbf{A}_{22}^{-1} \mathbf{C}_2^\top) \hat{\mathbf{S}}^{-1}, \quad \mathbf{T}_{33} = -(\mathbf{C} \mathbf{A}_{11}^{-1} \mathbf{C}^\top + \mathbf{C} \mathbf{A}_{11}^{-1} \mathbf{A}_{12} \mathbf{A}_{22}^{-1} \mathbf{C}_2^\top + \mathbf{C}_2 \mathbf{A}_{22}^{-1} \mathbf{C}_2^\top) \hat{\mathbf{S}}^{-1}.$$

In order to proceed further, we need the following lemma, whose proof can also be found in Appendix A.

**Lemma 5.** *The following identity holds:*

$$(66) \quad \gamma_1 \mathbf{C} \mathbf{A}_{11}^{-1} \mathbf{C}^\top \mathbf{W}^{-1} = \mathbf{I}_\ell - (\mathbf{I}_\ell + \gamma_1 \mathbf{C} \mathbf{A}_{11}^{-1} \mathbf{C}^\top \mathbf{W}^{-1})^{-1}.$$

Applying (66) to the preconditioned matrix in (65), we obtain the following result, whose proof is given in Appendix A.

**Lemma 6.** *Letting*

$$\begin{aligned} \mathbf{D} &= \gamma_2 \mathbf{C}_2^\top \mathbf{W}^{-1} (\mathbf{I}_\ell - (\mathbf{I}_\ell + \gamma_1 \mathbf{C} \mathbf{A}_{11}^{-1} \mathbf{C}^\top \mathbf{W}^{-1})^{-1}), \\ \mathbf{E} &= \mathbf{C}_2 \mathbf{A}_{22}^{-1}, \\ \mathbf{G} &= \mathbf{I}_\ell - \gamma_1 \mathbf{C}_2 \mathbf{A}_{22}^{-1} \mathbf{C}_2^\top \mathbf{W}^{-1}, \\ \mathbf{F} &= (\mathbf{I}_\ell + \gamma_1 \mathbf{C} \mathbf{A}_{11}^{-1} \mathbf{C}^\top \mathbf{W}^{-1})^{-1}, \end{aligned}$$

the right-preconditioned matrix can be written as:

$$(67) \quad \mathcal{A}_{\gamma_1, \gamma_2} \tilde{\mathcal{P}}_{\gamma_1, \gamma_2}^{-1} = \begin{bmatrix} \mathbf{I}_n & 0 & 0 \\ \mathbf{A}_{21} \mathbf{A}_{11}^{-1} & \mathbf{I}_m - \mathbf{D} \mathbf{E} & \mathbf{D} \mathbf{G} \left( \frac{1}{\gamma_1} \mathbf{W} \right) \hat{\mathbf{S}}^{-1} \\ \mathbf{C} \mathbf{A}_{11}^{-1} & -\mathbf{F} \mathbf{E} & (\mathbf{I}_\ell - \mathbf{F} \mathbf{G}) \left( -\frac{1}{\gamma_1} \mathbf{W} \right) \hat{\mathbf{S}}^{-1} \end{bmatrix}.$$

The foregoing lemma suggests the choice  $\hat{\mathbf{S}}^{-1} = -\gamma_1 \mathbf{W}^{-1}$ . This leads to the following theorem, which provides a characterization of the spectrum of the preconditioned system with the modified variant, and resembles the findings obtained in [17].

**Theorem 4** (Spectrum of preconditioned system with modified variant). *Let  $\hat{\mathbf{S}}^{-1} = -\gamma_1 \mathbf{W}^{-1}$ . We obtain*

$$(68) \quad \mathcal{A}_{\gamma_1, \gamma_2} \tilde{\mathcal{P}}_{\gamma_1, \gamma_2}^{-1} = \begin{bmatrix} \mathbf{I}_n & 0 & 0 \\ \mathbf{A}_{21} \mathbf{A}_{11}^{-1} & \mathbf{I}_m - \mathbf{D} \mathbf{E} & -\mathbf{D} \mathbf{G} \\ \mathbf{C} \mathbf{A}_{11}^{-1} & -\mathbf{F} \mathbf{E} & \mathbf{I}_\ell - \mathbf{F} \mathbf{G} \end{bmatrix}.$$

The matrix  $\mathcal{A}_{\gamma_1, \gamma_2} \tilde{\mathcal{P}}_{\gamma_1, \gamma_2}^{-1}$  has 1 as an eigenvalue of algebraic multiplicity at least  $n + m$ . The remaining eigenvalues are the non-unit eigenvalues of the matrix

$$(69) \quad \begin{bmatrix} \mathbf{I}_m - \mathbf{D} \mathbf{E} & -\mathbf{D} \mathbf{G} \\ -\mathbf{F} \mathbf{E} & \mathbf{I}_\ell - \mathbf{F} \mathbf{G} \end{bmatrix}.$$

*Proof.* Equality (68) immediately follows from (67) by substitution. Furthermore, the spectrum of  $\mathcal{A}_{\gamma_1, \gamma_2} \tilde{\mathcal{P}}_{\gamma_1, \gamma_2}^{-1}$  consists of the eigenvalue 1 of multiplicity  $n$ , plus the spectrum of the matrix

$$\begin{bmatrix} \mathbf{I}_m - \text{DE} & -\text{DG} \\ -\text{FE} & \mathbf{I}_\ell - \text{FG} \end{bmatrix} = \begin{bmatrix} \mathbf{I}_m & 0 \\ 0 & \mathbf{I}_\ell \end{bmatrix} - \begin{bmatrix} \text{DE} & \text{DG} \\ \text{FE} & \text{FG} \end{bmatrix}.$$

Observing that

$$(70) \quad \begin{bmatrix} \text{DE} & \text{DG} \\ \text{FE} & \text{FG} \end{bmatrix} = \begin{bmatrix} \text{D} \\ \text{F} \end{bmatrix} [\text{E} \quad \text{G}],$$

we have

$$\text{rank} \begin{bmatrix} \text{DE} & \text{DG} \\ \text{FE} & \text{FG} \end{bmatrix} \leq \min \left( \text{rank} \begin{bmatrix} \text{D} \\ \text{F} \end{bmatrix}, \text{rank} [\text{E} \quad \text{G}] \right) \leq \ell,$$

because  $\begin{bmatrix} \text{D} \\ \text{F} \end{bmatrix} \in \mathbb{R}^{(m+\ell) \times \ell}$  and  $[\text{E} \quad \text{G}] \in \mathbb{R}^{\ell \times (m+\ell)}$ . This implies that the matrix (69) has the eigenvalue 1 of multiplicity at least  $m$ . Therefore,  $\mathcal{A}_{\gamma_1, \gamma_2} \tilde{\mathcal{P}}_{\gamma_1, \gamma_2}^{-1}$  has 1 as an eigenvalue of algebraic multiplicity at least  $n + m$ .  $\square$

**6.1. Asymptotic behavior of remaining eigenvalues.** Similar to the case of the ideal preconditioner developed in Section 3, we set  $\mathbf{W} = \mathbf{M}^2$ . In this case, some observations can be made regarding the asymptotic behavior of the remaining  $\ell$  eigenvalues of matrix (69) that differ from 1. For the sake of exposition, and coherently with the setting of our numerical experiments, we consider the case  $\mathbf{C}_2 = \mathbf{M}$ , so that  $\mathbf{C}_2^T \mathbf{W}^{-1} \mathbf{C}_2 = \mathbf{I}_m$ . However, similar conclusions are expected to hold also in the more general scenario where  $\mathbf{C}_2$  is rectangular, as suggested by numerical tests with spaces  $V_{2,h} \neq \Lambda_h$ , which will be presented in Section 7. We omit the subscript in the identity matrix, since  $m = \ell$ .

As shown in Section 4, for the ideal AL preconditioner all the eigenvalues of the preconditioned matrix cluster towards 1 as  $\gamma \rightarrow \infty$ . This is not generally the case for the modified variants (59) and (61). However, the following result holds for the latter.

**Theorem 5** (Spectral convergence of the non-zero eigenvalues of the matrix (70)). *Let  $\mathbf{W} = \mathbf{M}^2$ , and let  $V_h$ ,  $V_{2,h}$ , and  $\Lambda_h$  be continuous Lagrangian finite element spaces. Then, the reciprocals of the non-zero eigenvalues of the matrix (70) converge to the eigenvalues of  $-\mathbf{L}\mathbf{A}_2$  as  $\gamma_1 \rightarrow \infty$  and  $\gamma_2 \rightarrow 0$ , where  $\mathbf{L} := \mathbf{M}^{-1} \mathbf{C} \mathbf{A}^{-1} \mathbf{C}^T \mathbf{M}^{-1}$ .*

*Proof.* By choosing  $\mathbf{W} = \mathbf{M}^2$  and selecting the finite element spaces so that  $\mathbf{C}_2 = \mathbf{M}$ , the matrices  $\text{D}$ ,  $\text{E}$ ,  $\text{G}$ , and  $\text{F}$  introduced in Lemma 6 can be rewritten as follows:

$$\begin{aligned} \text{D} &= \gamma_2 \mathbf{M}^{-1} (\mathbf{I} - (\mathbf{I} + \gamma_1 \mathbf{C} \mathbf{A}^{-1} \mathbf{C}^T \mathbf{M}^{-2})^{-1}), \\ \text{E} &= \mathbf{M} \mathbf{A}_{22}^{-1}, \\ \text{G} &= \mathbf{I} - \gamma_1 \mathbf{M} \mathbf{A}_{22}^{-1} \mathbf{M}^{-1}, \\ \text{F} &= (\mathbf{I} + \gamma_1 \mathbf{C} \mathbf{A}^{-1} \mathbf{C}^T \mathbf{M}^{-2})^{-1}. \end{aligned}$$

Note that all the necessary inverses exist. As observed in Theorem 4, the matrix (70) has rank at most  $\ell$ , and its non-zero eigenvalues coincide with those of the smaller matrix

$$[\text{E} \quad \text{G}] \begin{bmatrix} \text{D} \\ \text{F} \end{bmatrix} = \text{ED} + \text{GF}.$$

Substituting the expressions for  $\text{D}$ ,  $\text{E}$ ,  $\text{G}$ , and  $\text{F}$  yields:

$$\text{ED} + \text{GF} = \gamma_2 \mathbf{M} \mathbf{A}_{22}^{-1} \mathbf{M}^{-1} (\mathbf{I} - (\mathbf{I} + \gamma_1 \mathbf{C} \mathbf{A}^{-1} \mathbf{C}^T \mathbf{M}^{-2})^{-1}) + (\mathbf{I} - \gamma_1 \mathbf{M} \mathbf{A}_{22}^{-1} \mathbf{M}^{-1}) (\mathbf{I} + \gamma_1 \mathbf{C} \mathbf{A}^{-1} \mathbf{C}^T \mathbf{M}^{-2})^{-1}.$$

Using the fact that  $\mathbf{A}_{22} = \mathbf{A}_2 + \gamma_2 \mathbf{I}$  and performing some simple algebra, we obtain:

$$\text{ED} + \text{GF} = \gamma_2 \mathbf{M} (\mathbf{A}_2 + \gamma_2 \mathbf{I})^{-1} \mathbf{M}^{-1} - (\gamma_1 + \gamma_2) \mathbf{M} (\mathbf{A}_2 + \gamma_2 \mathbf{I})^{-1} \mathbf{M}^{-1} (\mathbf{I} + \gamma_1 \mathbf{C} \mathbf{A}^{-1} \mathbf{C}^T \mathbf{M}^{-2})^{-1} + (\mathbf{I} + \gamma_1 \mathbf{C} \mathbf{A}^{-1} \mathbf{C}^T \mathbf{M}^{-2})^{-1}.$$

Note that

$$(I + \gamma_1 CA^{-1}C^T M^{-2})^{-1} = (M(I + \gamma_1 M^{-1}CA^{-1}C^T M^{-1})M^{-1})^{-1} = M(I + \gamma_1 M^{-1}CA^{-1}C^T M^{-1})^{-1}M^{-1},$$

and substituting into the expression for ED + GF gives:

$$ED + GF = M\left(\gamma_2(A_2 + \gamma_2 I)^{-1} - (\gamma_1 + \gamma_2)(A_2 + \gamma_2 I)^{-1}(I + \gamma_1 M^{-1}CA^{-1}C^T M^{-1})^{-1} + (I + \gamma_1 M^{-1}CA^{-1}C^T M^{-1})^{-1}\right)M^{-1}.$$

Therefore, we can conclude that ED + GF is similar to the matrix

$$\gamma_2(A_2 + \gamma_2 I)^{-1} - (\gamma_1 + \gamma_2)(A_2 + \gamma_2 I)^{-1}(I + \gamma_1 M^{-1}CA^{-1}C^T M^{-1})^{-1} + (I + \gamma_1 M^{-1}CA^{-1}C^T M^{-1})^{-1}.$$

For the arguments that follow, it is convenient to consider the inverse of this matrix. By performing straightforward algebraic manipulations, we obtain that this inverse can be expressed as:

$$N := \left(L + \frac{1}{\gamma_1} I\right) \left(\gamma_2 \left(L + \frac{1}{\gamma_1} I\right) + \frac{1}{\gamma_1} (A_2 + \gamma_2 I) - \frac{\gamma_1 + \gamma_2}{\gamma_1} I\right)^{-1} (A_2 + \gamma_2 I),$$

where  $L := M^{-1}CA^{-1}C^T M^{-1}$ . It is evident that this matrix converges entrywise to  $-LA_2$  as  $\gamma_1 \rightarrow \infty$  and  $\gamma_2 \rightarrow 0$ .

To conclude the proof, we use the well-known fact that the eigenvalues of a square matrix depend continuously on its entries [47]. In other words, if we consider an infinite sequence of matrices  $N_k$  of dimensions  $m \times m$ , which converges to  $-LA_2$ , we can conclude that, among the up to  $m!$  possible ways of ordering the eigenvalues of the matrices  $N_{k_1}, N_{k_2}, \dots$  as a  $m$ -dimensional vector, there exists at least one ordering for each matrix such that the corresponding eigenvalue vectors converge to a vector whose components consist precisely of all the eigenvalues of  $-LA_2$ . Since ED + GF is similar to the inverse of N, this concludes the proof.  $\square$

**Remark 6** (Scaling considerations on  $LA_2$ ). *Notice that  $LA_2$  is the product of the symmetric and positive definite matrix  $M^{-1}CA^{-1}C^T M^{-1}$  and the symmetric positive semidefinite matrix  $A_2$ . Hence,  $LA_2$  is similar to a symmetric positive semidefinite matrix and therefore has real and positive eigenvalues, except for a single zero eigenvalue arising from the rank deficiency of  $A_2$ . Moreover, using well-known scaling properties of FEM matrices, we conclude that the entries of  $LA_2$  scale as  $\frac{\beta_2 - \beta}{\beta} \left(\frac{h_{\Omega_2}}{h_{\Omega}}\right)^2$ . Since the two meshes are assumed to be comparable, the ratio  $\frac{h_{\Omega_2}}{h_{\Omega}}$  is about one, while the ratio  $\frac{\beta_2 - \beta}{\beta}$  is larger than one thanks to our assumptions. Consequently, the spectrum of  $LA_2$  moves away from 1 as the jump increases.*

Theorem 5 provides insight into the behavior of the non-unit eigenvalues of the preconditioned matrix  $\mathcal{A}_{\gamma_1, \gamma_2} \tilde{\mathcal{P}}_{\gamma_1, \gamma_2}^{-1}$ , which coincide with the non-unit eigenvalues of the matrix (69). As observed in Theorem 4, the matrix (69) can be expressed as:

$$\begin{bmatrix} I - DE & -DG \\ -FE & I - FG \end{bmatrix} = \begin{bmatrix} I & 0 \\ 0 & I \end{bmatrix} - \begin{bmatrix} DE & DG \\ FE & FG \end{bmatrix},$$

implying that its eigenvalues are of the form  $1 - \lambda$ , where  $\lambda$  are the eigenvalues of (70). From Theorem 5, it follows that the non-zero eigenvalues of (70) tend to become real and negative, and to converge to zero as the jump increases, except for a single outlier that diverges to infinity. This behavior is advantageous, since the resulting eigenvalues  $1 - \lambda$  are tightly clustered around 1. This observation also explains the improved iteration counts observed for larger jumps in Section 7. Moreover, note that the presence of one outlier does not deteriorate the convergence behavior of GMRES.

It is also worth noting that a closer examination of the matrix N sheds light on why it is preferable to choose  $\gamma_1 \neq \gamma_2$  and in particular why it is convenient to select  $\gamma_1$  large and  $\gamma_2$  small, rather than using  $\gamma_1 = \gamma_2$ , which yields the same configuration analyzed in [17]. Indeed, if one considers the case  $\gamma_1 = \gamma_2$  and lets them tend either to 0 or to  $+\infty$ , the structure of the matrix N shows that certain terms become unbounded. Hence, the previous conclusions do not hold in this regime.

**6.2. Numerical test on remaining eigenvalues.** We validate the theoretical results by computing the eigenvalues of the 2-by-2 block

$$\begin{bmatrix} \mathbf{I}_m - \mathbf{DE} & -\mathbf{DG} \\ -\mathbf{FE} & \mathbf{I}_\ell - \mathbf{FG} \end{bmatrix}$$

when  $\gamma_1 \rightarrow \infty$  and  $\gamma_2 \rightarrow 0$ . To this aim, we consider the same configuration used in the experiments in Section 4.1. The size of the whole lower block associated with such a discretization is  $m + \ell = 81 + 81 = 162$ . As shown in the previous analysis,  $\lambda = 1$  is an eigenvalue of (69) with algebraic multiplicity  $m = 81$ . The spectrum is displayed in Figure 4. In addition to the expected 81 eigenvalues at 1, the rest of them progressively become real and move away from 0 as  $\gamma_1$  increases and  $\gamma_2$  decreases, in agreement with the fact that the spectrum of  $-\mathbf{LA}_2$  is real and negative. In the second and third plots the outlier is omitted for visualization reasons: when  $\gamma_1 = 10$  and  $\gamma_2 = 10^{-2}$ , the outlier is real and located at  $Re(\lambda) \approx 6.7$ , whereas for  $\gamma_1 = 10^2$  and  $\gamma_2 = 10^{-3}$  it is  $Re(\lambda) \approx 68.6$ .

Although we do not report the corresponding plots for larger jumps, the observed trend is that increasing the jump yields a tighter clustering around 1.

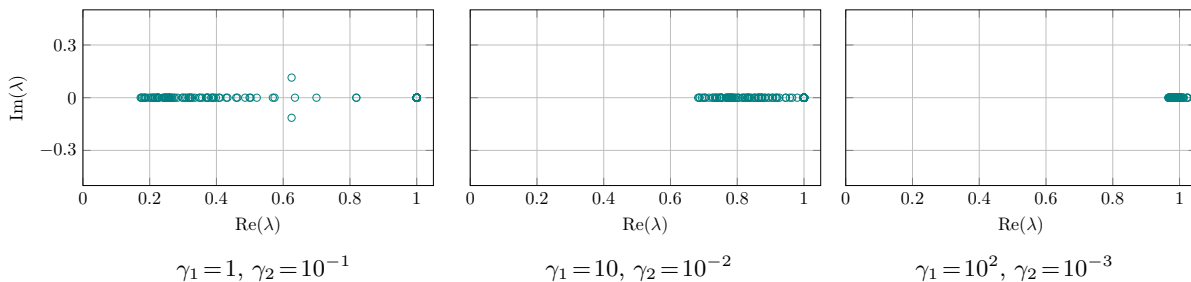


FIGURE 4.  $\beta = 1$ ,  $\beta_2 = 100$ . Spectrum of the lower block (6.2) for increasing  $\gamma_1$  and decreasing  $\gamma_2$ .

## 7. NUMERICAL EXPERIMENTS

In this section, we present numerical experiments aimed at evaluating the performance of the proposed augmented Lagrangian preconditioners for the augmented linear system of equations (60), stemming from the finite element discretization of Problem (1). All the experiments have been performed using the C++ finite element library DEAL.II [6, 7] and are available at the dedicated GitHub repository provided by the authors<sup>4</sup>. All computations have been carried out on a laptop equipped with an AMD Ryzen 9 PRO 7940HS processor and 64 GB of RAM, running Ubuntu 22.04 LTS.

Throughout the following examples, unless otherwise stated, we employ  $\mathcal{Q}^1$  Lagrangian finite elements for all finite element spaces  $V_h$ ,  $V_{2,h}$ , and  $\Lambda_h$ , on background and immersed meshes made of quadrilaterals or hexahedra. In particular, the background domain  $\Omega$  is always discretized using a structured mesh  $\mathcal{T}_h$ .

The outer Krylov subspace solver is set to FGMRES(30) with a restart every 30 iterations. All iterations start from a zero initial guess and are stopped when the relative residual norm is reduced below  $10^{-10}$ , or when its absolute value is below  $10^{-10}$ . We notice that we have chosen a rather strict tolerance compared to other papers analyzing preconditioners, which leads to higher iteration numbers. We have chosen this convergence criterion because it makes seeing trends easier due to the higher number of outer iterations. Right preconditioning is used in all cases. We will investigate AL and modified AL (MAL) preconditioners by varying *both* the immersed geometries  $\Omega_2$  and the size of the jump in the coefficients ( $\beta_2 - \beta$ ), while monitoring the iteration counts across simultaneous mesh refinement of both grids.

We will start by confirming the theoretical findings for the AL preconditioner  $\mathcal{P}_\gamma$  presented in Section 3. Then, we will analyze the performance of the modified variant, showing its practical advantages in terms of reduced computational cost. Following Section 3, the SPD matrix  $\mathbf{W}$  is set to  $\mathbf{M}^2$ . When considering the

<sup>4</sup>Available at [https://github.com/fdrmerc/fictitious\\_domain\\_AL\\_preconditioners](https://github.com/fdrmerc/fictitious_domain_AL_preconditioners).

modified AL preconditioner, sparse direct solvers could be used to solve the subsystems in (61) efficiently in 2D, while in the 3D case they quickly become prohibitively expensive, and inner iterative methods should be preferred in practice. For this reason, we will approximately solve the subsystems using the conjugate-gradient (CG) method preconditioned by one V-cycle of AMG with a loose inner tolerance set to  $10^{-2}$ . We adopt the TRILINOSML [45] implementation with parameters reported in Table B.1. Moreover, to facilitate the construction of the AMG preconditioner, we replace  $W$  with  $\text{diag}(W)$ , i.e., the matrix containing only the main diagonal of  $W$ , which avoids the computationally expensive triple matrix product involving the dense matrix  $W^{-1}$ . This modification is applied to both the system matrix and the preconditioner. We denote such inexact variant of the ideal modified AL preconditioner by  $\tilde{\mathcal{P}}_{\gamma_1, \gamma_2}^{\text{diag}}$ . Except where otherwise specified, the source terms are set to  $f = 1$  and  $f_2 = 2$ , while  $\beta = 1$ , and the value of the extended  $u$  on  $\partial\Omega$  is set to zero. In the forthcoming tables, the number of degrees of freedom for a finite dimensional space will be denoted by  $|\cdot|$ , e.g.  $|V_h|$ . Throughout the numerical experiments, we monitor only the inner iteration counts of the (1, 1)-block, which is particularly challenging due to the issues arising from the augmentation with the coupling matrix  $C$ .

**7.1. Validation of the AL preconditioner.** We first consider a uniform discretization of the domain  $\Omega_2 := [-0.14, 0.47]^2$ , immersed in the background domain  $\Omega := [-1, 1]^2$ , fixing  $\beta = 1$  and varying  $\beta_2$  from 10 to  $10^7$ . For each value of  $\beta_2$ , we report in Table 1A the number of outer iterations with the ideal AL preconditioner  $\mathcal{P}_\gamma$  upon mesh refinement. We invert all the diagonal blocks  $A_\gamma$  and  $W$  exactly. The augmentation parameter is set to  $\gamma = 10$ . We observe very low iteration counts, which are independent *both* of the refinement level, as well as of the size of the jump in the coefficients, confirming the observation in Remark 5 about parameter robustness.

We repeat the same experiment, this time considering a ball  $\Omega_2 := \mathcal{B}_{0.3}(0, 0)$  as immersed domain. The results with this geometry are shown in Table 1B, leading to identical conclusions in terms of iteration counts and robustness. Numerical solutions when  $\beta_2 = 10^7$  for both geometries are shown in Figure 5, showing in a wireframe representation the immersed domains.

A classical and appealing feature of AL-based preconditioners is that they do not require accurate solves for the augmented block for effectiveness [14, 15]. We have hence verified that identical FGMRES iterations are obtained when applying an inexact inversion of  $A_\gamma$  via a conjugate gradient method, preconditioned by a block-diagonal preconditioner with one AMG V-cycle on each diagonal block and a loose inner tolerance of  $10^{-2}$ . We will refer to this inexact variant as  $\mathcal{P}_\gamma^{\text{inexact}}$ , where again  $W$  is replaced by  $\text{diag}(W)$ . However, this inversion is far from efficient since the inner iterations grow unboundedly upon mesh refinement (exceeding an average of 70 PCG iterations for the finest discretization). The current lack of a  $\gamma$ -robust and mesh-independent geometric multigrid solver for  $A_\gamma$  in the fictitious domain setting represents the main computational bottleneck for this (unmodified) version of the AL preconditioner.

Iteration counts with $\mathcal{P}_\gamma$				Iteration counts with $\mathcal{P}_\gamma$			
DoF ( $ V_h  +  V_{2,h}  +  \Lambda_h $ )	$\beta_2 = 10$	$\beta_2 = 10^3$	$\beta_2 = 10^7$	DoF ( $ V_h  +  V_{2,h}  +  \Lambda_h $ )	$\beta_2 = 10$	$\beta_2 = 10^3$	$\beta_2 = 10^7$
289 + 25+25	8	8	8	289 + 8+8	4	3	3
1089 + 81+81	7	7	7	1089 + 25+25	7	7	7
4,225 + 289 + 289	6	7	7	4,225 + 89+89	7	7	7
16,641 + 1,089 + 1,089	6	6	6	16,641 + 337+337	7	7	7
66,049 + 4,225 + 4,225	5	5	5	66,049 + 1,313+1,313	6	6	6
263,169 + 16,641 + 16,641	4	5	5	263,169 + 5,185+5,185	6	6	6
1,050,625 + 66,049 + 66,049	4	4	4	1,050,625 + 20,609+20,609	5	5	5
4,198,401 + 263,169 + 263,169	4	4	4	4,198,401 + 82,177+82,177	5	5	5

(A) Immersed square.

(B) Immersed ball.

TABLE 1. Iteration counts with the ideal AL preconditioner  $\mathcal{P}_\gamma$ , varying the jump coefficient  $\beta_2$  across several refinement levels for the square and ball geometries.

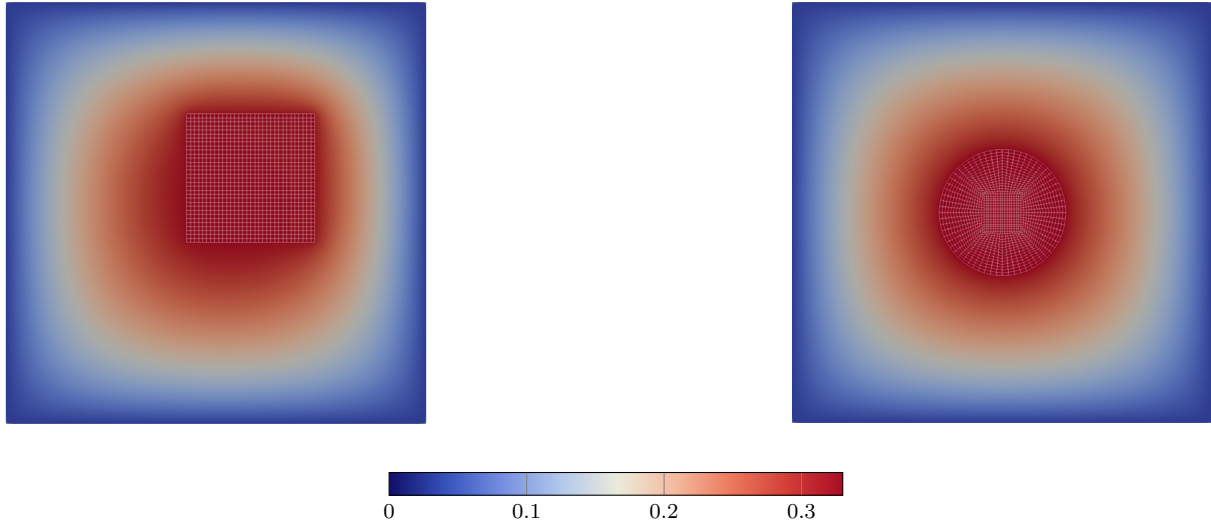


FIGURE 5. Numerical solutions when  $\beta_2 = 10^7$  for the square and ball geometries.

**7.2. Validation of the inexact modified AL preconditioner.** Having validated the ideal AL preconditioner and its inexact variant, we consider the inexact MAL preconditioner  $\tilde{\mathcal{P}}_{\gamma_1, \gamma_2}^{\text{diag}}$ , in which inner iterative methods and a diagonal approximation of  $W$  are employed. We repeat the same experiments for both geometries in the previous example, fixing  $\gamma_1 = 10$  and  $\gamma_2 = 10^{-2}$ . The results are shown in Table 2. Slightly higher iteration counts than in the unmodified case are observed, which are nevertheless independent of the refinement level and reasonably robust with respect to the jump in the coefficients. However, when  $\beta_2 = 10$ , we notice an increase in iteration counts. This is consistent with the observations made in Remark 6 about the better properties of the modified preconditioner for larger jumps. Between parentheses, we report the iteration counts when the parameter  $\gamma_2$  is taken to the lower value of  $10^{-3}$ , which provides consistent results with those for higher values of  $\beta_2$ . We have checked that using  $\gamma_2 = 10^{-3}$  for the other values of  $\beta_2$  gives lower outer iterations, but the gain is not as large as with  $\beta_2 = 10$ , since the spectrum is already more clustered when  $\beta_2 - \beta$  is large. For this reason, we will keep  $\gamma_2 = 10^{-2}$  in these regimes.

The last column shows the (average) number of inner conjugate-gradient iterations required for the approximate inversion of the  $(1, 1)$ -block of the preconditioner when  $\beta_2 = 10^7$ . We observe very low inner iteration counts upon mesh refinement, indicating that this modified variant might be a viable option to further reduce the computational cost of the AL preconditioner. Indeed, the gain in computational cost of the inexact MAL preconditioner with respect to the inexact AL preconditioner is quite significant, as indicated by the wall-clock time reported in Figure 6, where we show, in a log-log scale, the wall-clock time (in seconds) to solve the linear system for a sequence of refinement cycles when  $\beta_2 = 10^7$ . The curve for the modified approach lies well below that of the inexact AL preconditioner. Although it requires more outer iterations, the former yields the lowest computational times, thanks to the lower number of inner iterations. More precisely, for the finest refinement level,  $\mathcal{P}_\gamma^{\text{inexact}}$  takes about 300 seconds, while  $\tilde{\mathcal{P}}_{\gamma_1, \gamma_2}^{\text{diag}}$  needs 67 seconds. Compared to the unmodified variant,  $\tilde{\mathcal{P}}_{\gamma_1, \gamma_2}^{\text{diag}}$  gives a speed-up of a factor greater than four. A possible alternative would be to use  $\text{diag}(W)$  only in the preconditioner. This choice reduces the number of outer iterations but substantially increases the number of inner iterations, limiting its applicability due to the observed higher computational cost. Therefore, we omit it from the discussion. While a detailed comparison of the solvers is beyond the scope of this paper, we observe that these computational gains are representative.

**7.2.1. Comparison with a preconditioner from the literature.** We end the validation of our modified preconditioner by comparing in Table 3 the number of iterations of the inexact MAL preconditioner with those obtained using the block upper-triangular preconditioner introduced in [25] and extended in [2] to

FGMRES iteration counts with $\tilde{\mathcal{P}}_{\gamma_1, \gamma_2}^{\text{diag}}$				
DoF ( $ V_h  +  V_{2,h}  +  \Lambda_h $ )	$\beta_2 = 10$	$\beta_2 = 10^3$	$\beta_2 = 10^7$	Inner
289 + 25 + 25	16	17	17	2
1089 + 81 + 81	18 (17)	18	18	2
4,225 + 289 + 289	19 (17)	19	19	8
16,641 + 1,089 + 1,089	20 (16)	20	20	8
66,049 + 4,225 + 4,225	22 (16)	22	22	9
263,169 + 16,641 + 16,641	25 (18)	24	24	9
1,050,625 + 66,049 + 66,049	39 (19)	25	25	10
4,198,401 + 263,169 + 263,169	100 (28)	22	21	11

(A) Immersed square.

FGMRES iteration counts with $\tilde{\mathcal{P}}_{\gamma_1, \gamma_2}^{\text{diag}}$				
DoF ( $ V_h  +  V_{2,h}  +  \Lambda_h $ )	$\beta_2 = 10$	$\beta_2 = 10^3$	$\beta_2 = 10^7$	Inner
289 + 8 + 8	5	5	6	2
1089 + 25 + 25	10 (11)	10	10	2
4,225 + 89 + 89	16 (14)	16	16	8
16,641 + 337 + 337	16 (13)	16	16	8
66,049 + 1,313 + 1,313	19 (14)	18	18	9
263,169 + 5,185 + 5,185	20 (14)	19	18	9
1,050,625 + 20,609 + 20,609	23 (16)	21	21	10
4,198,401 + 82,177 + 82,177	36 (17)	21	21	11

(B) Immersed ball.

TABLE 2. Outer iteration counts for FGMRES preconditioned by  $\tilde{\mathcal{P}}_{\gamma_1, \gamma_2}^{\text{diag}}$ , varying the jump coefficient  $\beta_2$  across several refinement levels for the square (2A) and ball (2B) tests. The AL parameters are  $\gamma_1 = 10$ ,  $\gamma_2 = 10^{-2}$ . Value between parentheses indicate the iteration counts for  $\gamma_2 = 10^{-3}$ . The last column reports the average number of inner CG iterations to invert the (1,1)-block when  $\beta_2 = 10^7$ .

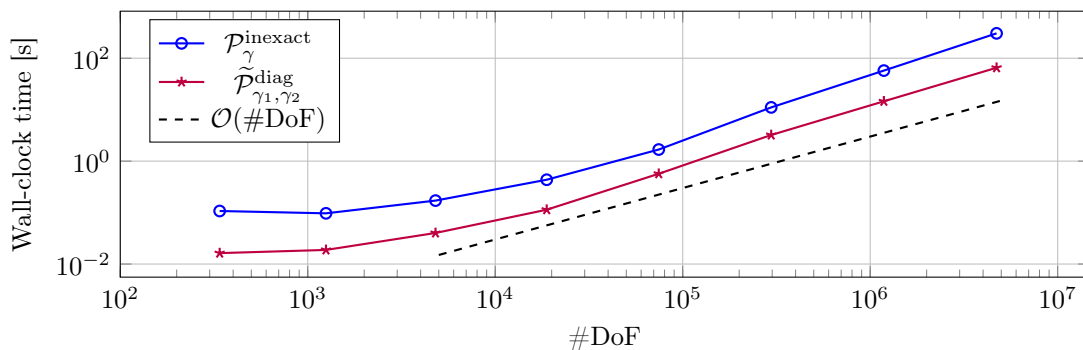


FIGURE 6. Comparison between the inexact AL  $\mathcal{P}_{\gamma}^{\text{inexact}}$  and MAL  $\tilde{\mathcal{P}}_{\gamma_1, \gamma_2}^{\text{diag}}$  preconditioners in terms of computational time for  $\beta_2 = 10^7$ , using the test case with the immersed square.

the elliptic-interface case. We mention that the latter requires the inversion of  $\mathbf{A}$  and of the two-by-two block<sup>5</sup>  $\begin{bmatrix} \mathbf{A}_2 & -\mathbf{C}_2^T \\ -\mathbf{C}_2 & 0 \end{bmatrix}$ . Since our interest is in the effectiveness of the preconditioners with respect to jumps in the coefficients, we consider direct inversion of these blocks and use a right-preconditioned GMRES(50) as outer solver, but we point out that multigrid-based inexact variants for these block solves are also possible in practice [2]. We consider again the ball  $\mathcal{B}_{0.3}(0,0)$  as immersed geometry, using a wider range of values for  $\beta_2$  compared to the previous examples, in order to investigate the robustness with respect to increasing coefficients jumps. Each table entry reports, as first element, the number of iterations of FGMRES preconditioned by  $\tilde{\mathcal{P}}_{\gamma_1, \gamma_2}^{\text{diag}}$ , and, as second element, the iterations of GMRES preconditioned by the block upper-triangular preconditioner in [25]. For the latter, a deterioration in the convergence is observed as the jump increases: for  $\beta_2 = 10^5$ , iteration counts displays a lack of robustness with respect to mesh-refinement, while for  $\beta_2 = 10^7$  GMRES fails to converge within 500 iterations. Conversely, the inexact MAL preconditioner maintains low iteration counts across all jumps and refinement levels. However, for moderate values of  $\beta_2$ , both approaches exhibit good iteration counts, which are robust in the mesh-sizes.

<sup>5</sup>The existence of this inverse follows from the ellipticity of  $\mathbf{A}_2$  in the kernel of  $\mathbf{C}_2$ , which is trivially satisfied when  $\mathbf{C}_2 = \mathbf{M}$  upon discretization. This has been shown to hold also when  $\mathbf{C}_2$  is not the standard mass matrix, for instance when using other stable pairs [2].

(F)GMRES iteration counts: $\tilde{\mathcal{P}}_{\gamma_1, \gamma_2}^{\text{diag}} / \text{block-triangular}$ [2]				
DoF ( $ V_h  +  V_{2,h}  +  \Lambda_h $ )	$\beta_2 = 10$	$\beta_2 = 10^3$	$\beta_2 = 10^5$	$\beta_2 = 10^7$
289 + 8 + 8	5/3	5/4	6/4	6/8
1,089 + 25 + 25	11/8	10/8	10/8	10/13
4,225 + 89 + 89	14/10	16/13	16/18	16/20
16,641 + 337 + 337	13/9	16/14	16/24	16/29
66,049 + 1,313 + 1,313	14/8	18/13	18/31	18/37
263,169 + 5,185 + 5,185	14/7	19/11	18/50	18/†
1,050,625 + 20,609 + 20,609	16/6	21/10	21/49	21/†

TABLE 3. Comparison between the inexact MAL preconditioner (with FGMRES) and the block upper-triangular preconditioner (with GMRES) from [2], applied to the immersed ball geometry. Symbol † indicates that GMRES did not converge within 500 iterations. When  $\beta_2 = 10$  we report the iteration counts for  $\gamma_2 = 10^{-3}$ , while other columns are obtained with  $\gamma_2 = 10^{-2}$ .

**7.3. More complex forcing term.** We now consider the numerical test presented in [59, Sect. 6]. The immersed domain is again  $\Omega_2 = \mathcal{B}_{0.3}(0, 0)$ , with forcing term  $f(x, y) = \sin(\pi x) + \tanh(y)$ . Neumann homogeneous boundary conditions are imposed on  $\partial\Omega$ . Numerical solutions for some selected values of the jump  $\beta_2 - \beta$  are shown in Figure 7, where the role played by the ratio  $\frac{\beta_2}{\beta}$  is visible: the higher it is, the higher are the gradient discontinuities across the immersed domain  $\Omega_2$ . We use the inexact modified AL-based preconditioner with  $\gamma_1 = 10$  and  $\gamma_2 = 10^{-2}$ , as in previous tests. Iteration counts using this configuration across mesh refinement are reported in Table 4. We observe robust iteration counts, essentially independent of the mesh-size and of the jump determined by the coefficient  $\beta_2$ . Consistently with the previous examples, for the lowest value of  $\beta_2$  a mild dependence on the mesh-size is observed, which is mitigated by decreasing the value of  $\gamma_2$  to  $10^{-3}$ . The (average) number of inner iterations when  $\beta_2 = 10^7$  is reported in the last column, where we observe them to be low and stable, confirming the previous trends.

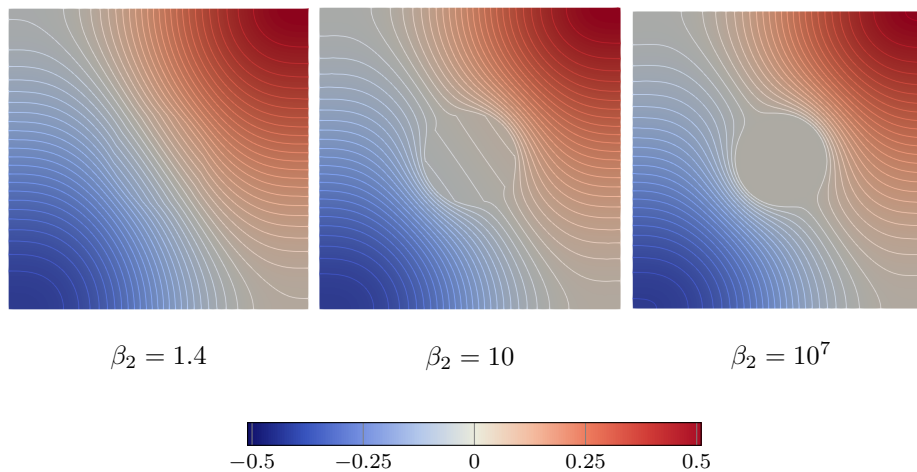


FIGURE 7. Numerical solutions  $u_h$  for different values of  $\beta_2$ . White lines are contour lines.

**7.4. Different finite elements.** We test the performance of the modified preconditioner when using different spaces than conforming  $\mathcal{Q}^1$  elements. As outlined in Remark 2, piecewise constant elements can be employed for the multiplier space  $\Lambda_h$ . Among them, we consider the  $\mathcal{Q}^1 - (\mathcal{Q}^1 + \mathfrak{B}) - \mathcal{Q}^0$  element, which was analyzed in [4]. With this choice for  $\Lambda_h$ , the mass matrix on the multiplier space, and hence  $W$ , are diagonal matrices by construction. On the other hand, the matrix  $C_2$  is now a rectangular (mass)

FGMRES iteration counts with $\tilde{\mathcal{P}}_{\gamma_1, \gamma_2}^{\text{diag}}$				
DoF ( $ V_h  +  V_{2,h}  +  \Lambda_h $ )	$\beta_2 = 10$	$\beta_2 = 10^3$	$\beta_2 = 10^7$	Inner
289 + 8 + 8	4 (5)	5	4	1
1089 + 25 + 25	9 (8)	9	8	1
4,225 + 89 + 89	15 (14)	15	15	6
16,641 + 337 + 337	15 (13)	14	15	6
66,049 + 1,313 + 1,313	16 (14)	16	16	6
263,169 + 5,185 + 5,185	16 (13)	15	15	7
1,050,625 + 20,609 + 20,609	19 (13)	15	15	8
4,198,401 + 82,177 + 82,177	31 (14)	14	14	9

TABLE 4. Outer iteration counts for FGMRES preconditioned by  $\tilde{\mathcal{P}}_{\gamma_1, \gamma_2}^{\text{diag}}$  when applied to Example 7.3, varying the jump coefficient  $\beta_2$  across several refinement levels. The AL parameters are  $\gamma_1 = 10$ ,  $\gamma_2 = 10^{-2}$ . Values between parentheses indicate the iteration counts for  $\gamma_2 = 10^{-3}$ . The last column reports the average number of inner iterations when  $\beta_2 = 10^7$ .

matrix. We repeat the same test cases as in Section 7.2, using the inexact MAL preconditioner with  $\gamma_1 = 10$  and  $\gamma_2 = 10^{-2}$ , for several refinement cycles and jumps in the coefficients. The results of such tests are in Table 5. Iteration counts for FGMRES are robust with respect to mesh refinements and jumps' size, confirming the effectiveness of the preconditioner also for other stable spaces. As observed in previous tests, for lower values of  $\beta_2$  a mild degradation is observed. Inner iteration counts for the (1, 1)-block when  $\beta_2 = 10^7$  remain low and stable, and are reported in the last column.

FGMRES iteration counts with $\tilde{\mathcal{P}}_{\gamma_1, \gamma_2}$					FGMRES iteration counts with $\tilde{\mathcal{P}}_{\gamma_1, \gamma_2}$				
DoF ( $ V_h  +  V_{2,h}  +  \Lambda_h $ )	$\beta_2 = 10$	$\beta_2 = 10^3$	$\beta_2 = 10^7$	Inner	DoF ( $ V_h  +  V_{2,h}  +  \Lambda_h $ )	$\beta_2 = 10$	$\beta_2 = 10^3$	$\beta_2 = 10^7$	Inner
289 + 41 + 16	13 (14)	14	10	1	289 + 13 + 5	6 (5)	5	5	1
1089 + 145 + 64	18 (18)	20	20	1	1089 + 45 + 20	6 (6)	6	6	1
4,225 + 545 + 256	19 (17)	19	19	5	4,225 + 169 + 80	15 (13)	15	15	8
16,641 + 2,113 + 1,024	18 (16)	19	19	6	16,641 + 657 + 320	17 (15)	19	19	8
66,049 + 8,321 + 4,096	19 (15)	19	19	7	66,049 + 2,593 + 1,280	19 (14)	19	19	9
263,169 + 33,025 + 16,384	21 (15)	20	20	7	263,169 + 10,305 + 5,120	20 (15)	21	21	10
1,050,625 + 131,585 + 65,536	23 (16)	22	22	8	1,050,625 + 41,089 + 20,480	23 (17)	23	23	10
4,198,401 + 525,313 + 262,144	38 (18)	23	23	8	4,198,401 + 164,097 + 81,920	26 (18)	26	25	11

(A) Immersed square.

(B) Immersed ball.

TABLE 5. FGMRES iteration counts for the modified preconditioner  $\tilde{\mathcal{P}}_{\gamma_1, \gamma_2}^{\text{diag}}$  applied to different geometries using the  $\mathcal{Q}^1 - (\mathcal{Q}^1 + \mathfrak{B}) - \mathcal{Q}^0$  element. Values between parentheses indicate the iteration counts for  $\gamma_2 = 10^{-3}$ .

**7.5. Three-dimensional test: linear elasticity.** We end this section by testing the inexact MAL preconditioner on a three-dimensional example. To the best of our knowledge, preconditioners proposed for the considered formulation (e.g., [2, 26, 65]) have thus far been applied exclusively to two-dimensional problems involving the Laplace operator. Instead of solving again the scalar model problem (3) in a higher dimension, we consider a three-dimensional linear elasticity example to test the strength of our approach in a more challenging setting. In our model, each subdomain is modeled as an isotropic and homogeneous material, allowing its mechanical behavior to be fully characterized by the corresponding Lamé constants [42]. The interested reader is referred to [5, 10] for the study of fictitious domain formulations applied to fiber-reinforced and multiscale materials.

Let  $\mu, \mu_2$  be the shear moduli in  $\Omega$  and  $\Omega_2$ , respectively, and  $\lambda, \lambda_2$  the first Lamé parameters. Consistently with the assumptions presented in Section 2, we assume  $\mu_2 > \mu > 0$  and  $\lambda_2 > \lambda > 0$ . We denote with  $\delta_\mu = \mu_2 - \mu$  and  $\delta_\lambda = \lambda_2 - \lambda$  the corresponding jumps. Vector-valued functions are indicated in boldface; thus, no ambiguity arises when  $\lambda$  denotes either a multiplier or a Lamé parameter. Adapting

the arguments from the previous sections to the vector-valued case, the fictitious domain formulation for the elasticity problem reads as follows.

**Problem 4** (Elasticity problem with FD-DLM). *Given  $\mathbf{f} \in [L^2(\Omega)]^3$ , find  $(\mathbf{u}, \mathbf{u}_2, \boldsymbol{\lambda}) \in V \times V_2 \times \Lambda$  such that*

$$\begin{aligned} 2\mu(\varepsilon(\mathbf{u}), \varepsilon(\mathbf{v}))_\Omega + \lambda(\operatorname{div} \mathbf{u}, \operatorname{div} \mathbf{v})_\Omega + c(\boldsymbol{\lambda}, \mathbf{v}|_{\Omega_2}) &= (\mathbf{f}, \mathbf{v})_\Omega & \forall \mathbf{v} \in V, \\ 2\delta_\mu(\varepsilon(\mathbf{u}_2), \varepsilon(\mathbf{v}_2))_{\Omega_2} + \delta_\lambda(\operatorname{div} \mathbf{u}_2, \operatorname{div} \mathbf{v}_2)_{\Omega_2} - c(\boldsymbol{\lambda}, \mathbf{v}_2) &= 0 & \forall \mathbf{v}_2 \in V_2, \\ c(\boldsymbol{\mu}, \mathbf{u}|_{\Omega_2} - \mathbf{u}_2) &= 0 & \forall \boldsymbol{\mu} \in \Lambda, \end{aligned}$$

where  $\varepsilon(\mathbf{u}) = \frac{1}{2}(\nabla \mathbf{u} + \nabla \mathbf{u}^\top)$  is the linearized strain tensor, and  $V = [H_0^1(\Omega)]^3$ ,  $V_2 = [H^1(\Omega_2)]^3$ ,  $\Lambda = [H^{-1}(\Omega_2)]^3$  are the vector-valued analogues of the spaces defined for the scalar problem.

It is straightforward to see that the algebraic formulation of Problem 4 is formally identical to the scalar one in problem (14), except that the matrices  $\mathbf{A}$  and  $\mathbf{A}_2$  correspond to bilinear forms associated with standard linear elasticity problems. Apart from the strain tensor term, the main difference with respect to the Laplace case is the presence of the additional "div-div" terms, which resembles the so-called "grad-div" stabilization used in standard AL preconditioners [56, 44]. However, it is crucial to observe that, in contrast to such approaches, this term naturally arises from the underlying physics rather than being artificially introduced. Hence, the setting is identical to the scalar case<sup>6</sup> discussed in Section 3, and the preconditioner can be applied without any modification. In spite of the presence of the "div-div" terms, augmenting only the second equation is insufficient and has a detrimental effect on the number of outer iterations, so both equations must be augmented.

The background domain is the cube  $\Omega = [-1.25, 1.25]^3$ , and the immersed domain  $\Omega_2$  is chosen as the rectangular box  $[-a, a] \times [-b, b] \times [-c, c]$ , with  $(a, b, c) = (0.65, 0.3, 0.4)$ . The initial configuration, displaying the immersed domain inside the background one, is shown in the left part of Figure 8. The displacement field  $\mathbf{u}: \Omega \rightarrow \mathbb{R}^3$  is set to zero on  $\partial\Omega$ , while  $\mathbf{f} = [2, 1, 1]^\top$  represents the body force. We test the inexact modified preconditioner  $\tilde{\mathcal{P}}_{\gamma_1, \gamma_2}^{\text{diag}}$ , fixing the augmentation parameters to  $\gamma_1 = 10$  and  $\gamma_2 = 10^{-2}$  as in previous two-dimensional tests, while iterations are stopped when the relative residual norm is reduced below  $10^{-6}$ . In our experiments, we vary the contrast between the Lamé parameters in the subdomains  $\Omega$  and  $\Omega_2$ , while monitoring the number of iterations under mesh refinement. We start with parameters  $(\mu, \mu_2) = (1, 10)$  and  $(\lambda, \lambda_2) = (2, 20)$ , corresponding to a tenfold ratio between the Lamé parameters. We then increase these ratios to 20 and 100, by considering  $(\mu, \mu_2) = (1, 20)$  and  $(\lambda, \lambda_2) = (2, 40)$ ,  $(\mu, \mu_2) = (1, 100)$  and  $(\lambda, \lambda_2) = (2, 200)$ , respectively. For each set of parameters, the materials exhibit a huge contrast in their Young's modulus  $E = 2\mu(1 + \nu)$ , which measures the material's stiffness under tensile or compressive force. This implies that the immersed body becomes increasingly stiffer than the surrounding medium. Hence, the higher the ratio, the less the immersed body deforms under the same applied force.

As shown in Table 6, the inexact MAL preconditioner delivers excellent outer iteration counts, largely independent of mesh refinement and ratios between the Lamé constants, while keeping moderate inner iteration counts.

A detailed visualization of the numerical solution  $\mathbf{u}_h$ , along with the reference and deformed configuration for the immersed body when  $(\mu, \mu_2) = (1, 20)$  and  $(\lambda, \lambda_2) = (2, 40)$ , is displayed in Figure 8.

<sup>6</sup>Indeed, the additional term  $(\operatorname{div} \mathbf{u}_2, \operatorname{div} \mathbf{v}_2)_{\Omega_2}$  does not remove the singularity from  $\mathbf{A}_2$ .

FGMRES iteration counts with $\tilde{\mathcal{P}}_{\gamma_1, \gamma_2}^{\text{diag}}$				
DoF ( $ V_h  +  V_{2,h}  +  \Lambda_h $ )	$\mu_2/\mu = \lambda_2/\lambda = 10$	$\mu_2/\mu = \lambda_2/\lambda = 20$	$\mu_2/\mu = \lambda_2/\lambda = 100$	Inner
$375 + 24 + 24$	25	26	26	1
$2187 + 81 + 81$	19	17	17	11
$14,739 + 375 + 375$	17	16	14	11
$107,811 + 2,187 + 2,187$	15	14	13	11
$823,875 + 14,739 + 14,739$	21	17	14	12

TABLE 6. FGMRES iteration counts for the modified preconditioner  $\tilde{\mathcal{P}}_{\gamma_1, \gamma_2}^{\text{diag}}$  applied to the linear elasticity example for different ratios of Lamé parameters between subdomains. Last column reports the average number of inner preconditioned CG iterations needed to approximately invert the (1,1)-block when the ratio between Lamé constants is 20.

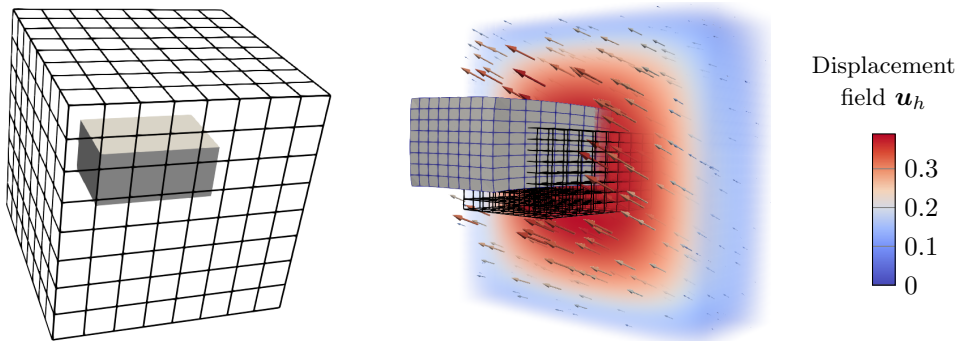


FIGURE 8. Left: background domain (black lines) containing the immersed domain  $\Omega_2$ . Right: detail of the numerical solution obtained with  $\mu_2/\mu = \lambda_2/\lambda = 20$ . Arrows indicate the computed displacement field  $\mathbf{u}_h$ , while its magnitude is shown in the background domain using a color map with opacity. The black wireframe depicts the undeformed (reference) configuration of the immersed body, whereas the gray surface is the deformed one.

## 8. CONCLUSIONS

We have presented a novel augmented Lagrangian-based preconditioner to accelerate the convergence of iterative solvers for saddle point systems arising from the finite element discretization of elliptic interface problems using a fictitious domain approach. We have derived ideal and modified variants of the preconditioner. The modified version, owing to its block-triangular structure, is particularly suitable for practical applications as it enables the use of off-the-shelf solvers from established high-performance libraries. A spectral analysis has been performed for both variants. We have shown, through extensive numerical experiments with different configurations, that the proposed preconditioners are robust with respect to mesh sizes and jumps in the coefficients. Ongoing work aims to extend the preconditioning strategy presented in this paper to fluid-structure interaction problems and to develop tailored solvers for the efficient inversion of the augmented (1,1)-block.

## ACKNOWLEDGMENTS

MB acknowledges partial support from grant MUR PRIN 2022 No. 20227PCCKZ (“Low Rank Structures and Numerical Methods in Matrix and Tensor Computations and their Applications”). LH and MF acknowledge partial support from grant MUR PRIN 2022 No. 2022WKWZA8 (“Immersed methods for multiscale and multiphysics problems (IMMEDIATE)”), and the support of the European Research Council (ERC) under the European Union’s Horizon 2020 research and innovation programme (call HORIZON-EUROHPC-JU-2023-COE-03, grant agreement No. 101172493 “dealii-X”). The authors are

members of Gruppo Nazionale per il Calcolo Scientifico (GNCS) of Istituto Nazionale di Alta Matematica (INdAM).

#### APPENDIX A.

In this appendix we give the proofs of the lemmas in Section 6.

**Proof of Lemma 4.** Let

$$\mathbf{A}_{\gamma_1, \gamma_2} := \begin{bmatrix} \mathbf{A} + \gamma \mathbf{C}^\top \mathbf{W}^{-1} \mathbf{C} & -\gamma_1 \mathbf{C}^\top \mathbf{W}^{-1} \mathbf{C}_2 \\ -\gamma_2 \mathbf{C}_2^\top \mathbf{W}^{-1} \mathbf{C} & \mathbf{A}_2 + \gamma \mathbf{C}_2^\top \mathbf{W}^{-1} \mathbf{C}_2 \end{bmatrix}$$

and

$$\tilde{\mathbf{A}}_{\gamma_1, \gamma_2} := \begin{bmatrix} \mathbf{A} + \gamma \mathbf{C}^\top \mathbf{W}^{-1} \mathbf{C} & -\gamma_1 \mathbf{C}^\top \mathbf{W}^{-1} \mathbf{C}_2 \\ 0 & \mathbf{A}_2 + \gamma \mathbf{C}_2^\top \mathbf{W}^{-1} \mathbf{C}_2 \end{bmatrix}.$$

Using the factorization in (64), we have

$$\begin{aligned} \mathcal{A}_{\gamma_1, \gamma_2} \tilde{\mathcal{P}}_{\gamma_1, \gamma_2}^{-1} &= \begin{bmatrix} \mathbf{A}_{\gamma_1, \gamma_2} & \mathbf{B}^\top \\ \mathbf{B} & \mathbf{0} \end{bmatrix} \begin{bmatrix} \tilde{\mathbf{A}}_{\gamma_1, \gamma_2}^{-1} & \mathbf{0} \\ \mathbf{0} & \mathbf{I}_\ell \end{bmatrix} \begin{bmatrix} \mathbf{I}_{n+m} & \mathbf{B}^\top \\ \mathbf{0} & -\mathbf{I}_\ell \end{bmatrix} \begin{bmatrix} \mathbf{I}_{n+m} & \mathbf{0} \\ \mathbf{0} & -\hat{\mathbf{S}}^{-1} \end{bmatrix} \\ &= \begin{bmatrix} \mathbf{A}_{\gamma_1, \gamma_2} \tilde{\mathbf{A}}_{\gamma_1, \gamma_2}^{-1} & -(\mathbf{A}_{\gamma_1, \gamma_2} \tilde{\mathbf{A}}_{\gamma_1, \gamma_2}^{-1} - \mathbf{I}_{n+m}) \mathbf{B}^\top \hat{\mathbf{S}}^{-1} \\ \mathbf{B} \tilde{\mathbf{A}}_{\gamma_1, \gamma_2}^{-1} & -\mathbf{B} \tilde{\mathbf{A}}_{\gamma_1, \gamma_2}^{-1} \mathbf{B}^\top \hat{\mathbf{S}}^{-1} \end{bmatrix} \end{aligned}$$

First, we observe that the inverse of  $\tilde{\mathbf{A}}_{\gamma_1, \gamma_2}$  is

$$\tilde{\mathbf{A}}_{\gamma_1, \gamma_2}^{-1} = \begin{bmatrix} \mathbf{A}_{11}^{-1} & -\mathbf{A}_{11}^{-1} \mathbf{A}_{12} \mathbf{A}_{22}^{-1} \\ \mathbf{0} & \mathbf{A}_{22}^{-1} \end{bmatrix}.$$

The (1, 1) block of  $\mathcal{A}_{\gamma_1, \gamma_2} \tilde{\mathcal{P}}_{\gamma_1, \gamma_2}^{-1}$  is

$$\mathbf{A}_{\gamma_1, \gamma_2} \tilde{\mathbf{A}}_{\gamma_1, \gamma_2}^{-1} = \begin{bmatrix} \mathbf{A}_{11} & \mathbf{A}_{12} \\ \mathbf{A}_{21} & \mathbf{A}_{22} \end{bmatrix} \begin{bmatrix} \mathbf{A}_{11}^{-1} & -\mathbf{A}_{11}^{-1} \mathbf{A}_{12} \mathbf{A}_{22}^{-1} \\ \mathbf{0} & \mathbf{A}_{22}^{-1} \end{bmatrix} = \begin{bmatrix} \mathbf{I}_n & \mathbf{0} \\ \mathbf{A}_{21} \mathbf{A}_{11}^{-1} & \mathbf{I}_m - \mathbf{A}_{21} \mathbf{A}_{11}^{-1} \mathbf{A}_{12} \mathbf{A}_{22}^{-1} \end{bmatrix}.$$

The (1, 2), (2, 1), and (2, 2) blocks are, respectively,

$$\begin{aligned} -(\mathbf{A}_{\gamma_1, \gamma_2} \tilde{\mathbf{A}}_{\gamma_1, \gamma_2}^{-1} - \mathbf{I}_{n+m}) \mathbf{B}^\top \hat{\mathbf{S}}^{-1} &= - \begin{bmatrix} \mathbf{0} & \mathbf{0} \\ \mathbf{A}_{21} \mathbf{A}_{11}^{-1} & -\mathbf{A}_{21} \mathbf{A}_{11}^{-1} \mathbf{A}_{12} \mathbf{A}_{22}^{-1} \end{bmatrix} \begin{bmatrix} \mathbf{C}^\top \\ -\mathbf{C}_2^\top \end{bmatrix} \hat{\mathbf{S}}^{-1} \\ (71) \qquad \qquad \qquad &= \begin{bmatrix} \mathbf{0} \\ (-\mathbf{A}_{21} \mathbf{A}_{11}^{-1} \mathbf{C}^\top - \mathbf{A}_{21} \mathbf{A}_{11}^{-1} \mathbf{A}_{12} \mathbf{A}_{22}^{-1} \mathbf{C}_2^\top) \hat{\mathbf{S}}^{-1} \end{bmatrix}, \end{aligned}$$

$$\begin{aligned} \mathbf{B} \tilde{\mathbf{A}}_{\gamma_1, \gamma_2}^{-1} &= [\mathbf{C} \quad -\mathbf{C}_2] \begin{bmatrix} \mathbf{A}_{11}^{-1} & -\mathbf{A}_{11}^{-1} \mathbf{A}_{12} \mathbf{A}_{22}^{-1} \\ \mathbf{0} & \mathbf{A}_{22}^{-1} \end{bmatrix} \\ (72) \qquad \qquad \qquad &= [\mathbf{C} \mathbf{A}_{11}^{-1} \quad -\mathbf{C} \mathbf{A}_{11}^{-1} \mathbf{A}_{12} \mathbf{A}_{22}^{-1} - \mathbf{C}_2 \mathbf{A}_{22}^{-1}], \end{aligned}$$

$$\begin{aligned}
(73) \quad -\tilde{\mathbf{B}}\tilde{\mathcal{A}}_{\gamma_1, \gamma_2}^{-1} \mathbf{B}^T \hat{\mathbf{S}}^{-1} &= -\begin{bmatrix} \mathbf{C} & -\mathbf{C}_2 \end{bmatrix} \begin{bmatrix} \mathbf{A}_{11}^{-1} & -\mathbf{A}_{11}^{-1} \mathbf{A}_{12} \mathbf{A}_{22}^{-1} \\ 0 & \mathbf{A}_{22}^{-1} \end{bmatrix} \begin{bmatrix} \mathbf{C}^T \\ -\mathbf{C}_2^T \end{bmatrix} \hat{\mathbf{S}}^{-1} \\
&= -\left( \mathbf{C} \mathbf{A}_{11}^{-1} \mathbf{C}^T + \mathbf{C} \mathbf{A}_{11}^{-1} \mathbf{A}_{12} \mathbf{A}_{22}^{-1} \mathbf{C}_2^T + \mathbf{C}_2 \mathbf{A}_{22}^{-1} \mathbf{C}_2^T \right) \hat{\mathbf{S}}^{-1}.
\end{aligned}$$

Plugging the above expressions into the expression for  $\mathcal{A}_{\gamma_1, \gamma_2} \tilde{\mathcal{P}}_{\gamma_1, \gamma_2}^{-1}$  gives (65).  $\square$

**Proof of Lemma 5.** Applying the Sherman-Morrison-Woodbury matrix identity

$$(\mathbf{Y} + \mathbf{UZV})^{-1} = \mathbf{Y}^{-1} - \mathbf{Y}^{-1} \mathbf{U} (\mathbf{Z}^{-1} + \mathbf{VY}^{-1} \mathbf{U})^{-1} \mathbf{VY}^{-1},$$

to  $\mathbf{A}_{11}^{-1} = (\mathbf{A} + \gamma_1 \mathbf{C}^T \mathbf{W}^{-1} \mathbf{C})^{-1}$  gives

$$\mathbf{A}_{11}^{-1} = \mathbf{A}^{-1} - \mathbf{A}^{-1} \mathbf{C}^T (\gamma_1^{-1} \mathbf{W} + \mathbf{C} \mathbf{A}^{-1} \mathbf{C}^T)^{-1} \mathbf{C} \mathbf{A}^{-1}.$$

Thus we have:

$$\begin{aligned}
\mathbf{C} \mathbf{A}_{11}^{-1} \mathbf{C}^T &= \mathbf{C} \left( \mathbf{A}^{-1} - \mathbf{A}^{-1} \mathbf{C}^T (\gamma_1^{-1} \mathbf{W} + \mathbf{C} \mathbf{A}^{-1} \mathbf{C}^T)^{-1} \mathbf{C} \mathbf{A}^{-1} \right) \mathbf{C}^T \\
&= \mathbf{C} \mathbf{A}^{-1} \mathbf{C}^T \left( \mathbf{I}_\ell - (\gamma_1^{-1} \mathbf{W} + \mathbf{C} \mathbf{A}^{-1} \mathbf{C}^T)^{-1} \mathbf{C} \mathbf{A}^{-1} \mathbf{C}^T \right) \\
&= \mathbf{C} \mathbf{A}^{-1} \mathbf{C}^T \left( \mathbf{I}_\ell - (\gamma_1^{-1} \mathbf{W} + \mathbf{C} \mathbf{A}^{-1} \mathbf{C}^T)^{-1} (\mathbf{C} \mathbf{A}^{-1} \mathbf{C}^T + \gamma_1^{-1} \mathbf{W} - \gamma_1^{-1} \mathbf{W}) \right) \\
&= \mathbf{C} \mathbf{A}^{-1} \mathbf{C}^T \left( \mathbf{I}_\ell - \mathbf{I}_\ell + (\gamma_1^{-1} \mathbf{W} + \mathbf{C} \mathbf{A}^{-1} \mathbf{C}^T)^{-1} \gamma_1^{-1} \mathbf{W} \right) \\
&= \mathbf{C} \mathbf{A}^{-1} \mathbf{C}^T (\gamma_1^{-1} \mathbf{W} + \mathbf{C} \mathbf{A}^{-1} \mathbf{C}^T)^{-1} \gamma_1^{-1} \mathbf{W} \\
&= (\mathbf{C} \mathbf{A}^{-1} \mathbf{C}^T + \gamma_1^{-1} \mathbf{W} - \gamma_1^{-1} \mathbf{W}) (\gamma_1^{-1} \mathbf{W} + \mathbf{C} \mathbf{A}^{-1} \mathbf{C}^T)^{-1} \gamma_1^{-1} \mathbf{W} \\
&= (\mathbf{I}_\ell - \gamma_1^{-1} \mathbf{W} (\gamma_1^{-1} \mathbf{W} + \mathbf{C} \mathbf{A}^{-1} \mathbf{C}^T)^{-1}) \gamma_1^{-1} \mathbf{W} \\
&= \gamma_1^{-1} \mathbf{W} - \gamma_1^{-1} \mathbf{W} (\gamma_1^{-1} \mathbf{W} + \mathbf{C} \mathbf{A}^{-1} \mathbf{C}^T)^{-1} \gamma_1^{-1} \mathbf{W}.
\end{aligned}$$

Multiplying by  $\gamma_1 \mathbf{W}^{-1}$  gives

$$\begin{aligned}
\gamma_1 \mathbf{C} \mathbf{A}_{11}^{-1} \mathbf{C}^T \mathbf{W}^{-1} &= \mathbf{I}_\ell - \gamma_1^{-1} \mathbf{W} (\gamma_1^{-1} \mathbf{W} + \mathbf{C} \mathbf{A}^{-1} \mathbf{C}^T)^{-1} \\
&= \mathbf{I}_\ell - \left( (\gamma_1^{-1} \mathbf{W} + \mathbf{C} \mathbf{A}^{-1} \mathbf{C}^T) (\gamma_1^{-1} \mathbf{W})^{-1} \right)^{-1} \\
&= \mathbf{I}_\ell - \left( \mathbf{I}_\ell + \gamma_1 \mathbf{C} \mathbf{A}^{-1} \mathbf{C}^T \mathbf{W}^{-1} \right)^{-1}.
\end{aligned}$$

We complete the proof by observing that all necessary inverses exist. In our system,  $\mathbf{A}$  is symmetric positive definite. Therefore, since  $\mathbf{C}$  has full row-rank,  $\mathbf{C} \mathbf{A}^{-1} \mathbf{C}^T$  is also SPD, and  $\mathbf{I}_\ell + \gamma_1 \mathbf{C} \mathbf{A}^{-1} \mathbf{C}^T \mathbf{W}^{-1}$  is necessarily invertible. Note that in the Oseen problem analyzed in [17],  $\mathbf{A}_2$  is invertible, therefore the same identity (66) is valid also for  $\mathbf{A}_{22}^{-1}$ . In our case, on the other hand,  $\mathbf{A}_2$  is singular (cf. Remark 1).

**Proof of Lemma 6.** From Lemma 4 we know that

$$\mathcal{A}_{\gamma_1, \gamma_2} \tilde{\mathcal{P}}_{\gamma_1, \gamma_2}^{-1} = \begin{bmatrix} \mathbf{I}_n & 0 & 0 \\ \mathbf{A}_{21} \mathbf{A}_{11}^{-1} & \mathbf{I}_m - \mathbf{A}_{21} \mathbf{A}_{11}^{-1} \mathbf{A}_{12} \mathbf{A}_{22}^{-1} & (-\mathbf{A}_{21} \mathbf{A}_{11}^{-1} \mathbf{C}^T - \mathbf{A}_{21} \mathbf{A}_{11}^{-1} \mathbf{A}_{12} \mathbf{A}_{22}^{-1} \mathbf{C}_2^T) \hat{\mathbf{S}}^{-1} \\ \mathbf{C} \mathbf{A}_{11}^{-1} & -\mathbf{C} \mathbf{A}_{11}^{-1} \mathbf{A}_{12} \mathbf{A}_{22}^{-1} - \mathbf{C}_2 \mathbf{A}_{22}^{-1} & -(\mathbf{C} \mathbf{A}_{11}^{-1} \mathbf{C}^T + \mathbf{C} \mathbf{A}_{11}^{-1} \mathbf{A}_{12} \mathbf{A}_{22}^{-1} \mathbf{C}_2^T + \mathbf{C}_2 \mathbf{A}_{22}^{-1} \mathbf{C}_2^T) \hat{\mathbf{S}}^{-1} \end{bmatrix}.$$

- First, we consider the (2,2)-block. Using the definitions of  $A_{21}$  and  $A_{12}$ , together with (66), we obtain

$$\begin{aligned}
\mathbf{I}_m - A_{21}A_{11}^{-1}A_{12}A_{22}^{-1} &= \mathbf{I}_m - (-\gamma_2\mathbf{C}_2^T\mathbf{W}^{-1}\mathbf{C})A_{11}^{-1}(-\gamma_1\mathbf{C}^T\mathbf{W}^{-1}\mathbf{C}_2)A_{22}^{-1} \\
&= \mathbf{I}_m - \gamma_2\mathbf{C}_2^T\mathbf{W}^{-1}(\gamma_1\mathbf{C}A_{11}^{-1}\mathbf{C}^T\mathbf{W}^{-1})\mathbf{C}_2A_{22}^{-1} \\
&= \mathbf{I}_m - \gamma_2\mathbf{C}_2^T\mathbf{W}^{-1}\left(\mathbf{I}_\ell - (\mathbf{I}_\ell + \gamma_1\mathbf{C}A^{-1}\mathbf{C}^T\mathbf{W}^{-1})^{-1}\right)\mathbf{C}_2A_{22}^{-1} \\
&= \mathbf{I}_m - \mathbf{D}\mathbf{E}
\end{aligned}$$

with

$$\mathbf{D} = \gamma_2\mathbf{C}_2^T\mathbf{W}^{-1}\left(\mathbf{I}_\ell - (\mathbf{I}_\ell + \gamma_1\mathbf{C}A^{-1}\mathbf{C}^T\mathbf{W}^{-1})^{-1}\right), \quad \mathbf{E} = \mathbf{C}_2A_{22}^{-1}.$$

- For the (2,3)-block, we have

$$\begin{aligned}
(-A_{21}A_{11}^{-1}\mathbf{C}^T - A_{21}A_{11}^{-1}A_{12}A_{22}^{-1}\mathbf{C}_2^T)\widehat{\mathbf{S}}^{-1} &= \left(\gamma_2\mathbf{C}_2^T\mathbf{W}^{-1}\mathbf{C}A_{11}^{-1}\mathbf{C}^T - \gamma_2\mathbf{C}_2^T\mathbf{W}^{-1}\mathbf{C}A_{11}^{-1}\gamma_1\mathbf{C}^T\mathbf{W}^{-1}\mathbf{C}_2A_{22}^{-1}\mathbf{C}_2^T\right)\widehat{\mathbf{S}}^{-1} \\
&= \gamma_2\mathbf{C}_2^T\mathbf{W}^{-1}\mathbf{C}A_{11}^{-1}\mathbf{C}^T\left(\mathbf{I}_\ell - \gamma_1\mathbf{W}^{-1}\mathbf{C}_2A_{22}^{-1}\mathbf{C}_2^T\right)\widehat{\mathbf{S}}^{-1} \\
&= \gamma_2\mathbf{C}_2^T\mathbf{W}^{-1}\mathbf{C}A_{11}^{-1}\mathbf{C}^T(\gamma_1\mathbf{W}^{-1})\left(\frac{1}{\gamma_1}\mathbf{W} - \mathbf{C}_2A_{22}^{-1}\mathbf{C}_2^T\right)\widehat{\mathbf{S}}^{-1} \\
&= \gamma_2\mathbf{C}_2^T\mathbf{W}^{-1}\mathbf{C}A_{11}^{-1}\mathbf{C}^T(\gamma_1\mathbf{W}^{-1})\left(\mathbf{I}_\ell - \gamma_1\mathbf{C}_2A_{22}^{-1}\mathbf{C}_2^T\mathbf{W}^{-1}\right)\left(\frac{1}{\gamma_1}\mathbf{W}\right)\widehat{\mathbf{S}}^{-1} \\
&= \gamma_2\mathbf{C}_2^T\mathbf{W}^{-1}\left(\gamma_1\mathbf{C}A_{11}^{-1}\mathbf{C}^T\mathbf{W}^{-1}\right)\left(\mathbf{I}_\ell - \gamma_1\mathbf{C}_2A_{22}^{-1}\mathbf{C}_2^T\mathbf{W}^{-1}\right)\left(\frac{1}{\gamma_1}\mathbf{W}\right)\widehat{\mathbf{S}}^{-1} \\
&= \gamma_2\mathbf{C}_2^T\mathbf{W}^{-1}\left(\mathbf{I}_\ell - (\mathbf{I}_\ell + \gamma_1\mathbf{C}A^{-1}\mathbf{C}^T\mathbf{W}^{-1})^{-1}\right)\left(\mathbf{I}_\ell - \gamma_1\mathbf{C}_2A_{22}^{-1}\mathbf{C}_2^T\mathbf{W}^{-1}\right)\left(\frac{1}{\gamma_1}\mathbf{W}\right)\widehat{\mathbf{S}}^{-1} \\
&= \mathbf{D}\mathbf{G}\left(\frac{1}{\gamma_1}\mathbf{W}\right)\widehat{\mathbf{S}}^{-1},
\end{aligned}$$

where

$$\mathbf{G} = \mathbf{I}_\ell - \gamma_1\mathbf{C}_2A_{22}^{-1}\mathbf{C}_2^T\mathbf{W}^{-1}.$$

- Next, for the (3,2)-block we have

$$\begin{aligned}
-\mathbf{C}A_{11}^{-1}A_{12}A_{22}^{-1} - \mathbf{C}_2A_{22}^{-1} &= \mathbf{C}A_{11}^{-1}\gamma_1\mathbf{C}^T\mathbf{W}^{-1}\mathbf{C}_2A_{22}^{-1} - \mathbf{C}_2A_{22}^{-1} \\
&= \left(\mathbf{C}A_{11}^{-1}\gamma_1\mathbf{C}^T\mathbf{W}^{-1} - \mathbf{I}_\ell\right)\mathbf{C}_2A_{22}^{-1} \\
&= \left(\mathbf{I}_\ell - \left(\mathbf{I}_\ell + \gamma_1\mathbf{C}A^{-1}\mathbf{C}^T\mathbf{W}^{-1}\right)^{-1} - \mathbf{I}_\ell\right)\mathbf{C}_2A_{22}^{-1} \\
&= -\left(\mathbf{I}_\ell + \gamma_1\mathbf{C}A^{-1}\mathbf{C}^T\mathbf{W}^{-1}\right)^{-1}\mathbf{C}_2A_{22}^{-1} \\
&= -\mathbf{F}\mathbf{E},
\end{aligned}$$

with

$$\mathbf{F} = \left(\mathbf{I}_\ell + \gamma_1\mathbf{C}A^{-1}\mathbf{C}^T\mathbf{W}^{-1}\right)^{-1}.$$

- Finally, the (3,3)-block:

$$\begin{aligned}
& -\left(\mathbf{CA}_{11}^{-1}\mathbf{C}^T + \mathbf{CA}_{11}^{-1}\mathbf{A}_{12}\mathbf{A}_{22}^{-1}\mathbf{C}_2^T + \mathbf{C}_2\mathbf{A}_{22}^{-1}\mathbf{C}_2^T\right)\widehat{\mathbf{S}}^{-1} \\
& = -\left(\mathbf{CA}_{11}^{-1}\mathbf{C}^T + \mathbf{C}_2\mathbf{A}_{22}^{-1}\mathbf{C}_2^T - \mathbf{CA}_{11}^{-1}\gamma_1\mathbf{C}^T\mathbf{W}^{-1}\mathbf{C}_2\mathbf{A}_{22}^{-1}\mathbf{C}_2^T\right)(\gamma_1\mathbf{W}^{-1})(\gamma_1\mathbf{W}^{-1})^{-1}\widehat{\mathbf{S}}^{-1} \\
& = -\left(\gamma_1\mathbf{CA}_{11}^{-1}\mathbf{C}^T\mathbf{W}^{-1} + \gamma_1\mathbf{C}_2\mathbf{A}_{22}^{-1}\mathbf{C}_2^T\mathbf{W}^{-1} - \gamma_1\mathbf{CA}_{11}^{-1}\gamma_1\mathbf{C}^T\mathbf{W}^{-1}\mathbf{C}_2\mathbf{A}_{22}^{-1}\mathbf{C}_2^T\mathbf{W}^{-1}\right)(\gamma_1\mathbf{W}^{-1})^{-1}\widehat{\mathbf{S}}^{-1} \\
& = -\left(\mathbf{I}_\ell - (\mathbf{I}_\ell - \gamma_1\mathbf{CA}_{11}^{-1}\mathbf{C}^T\mathbf{W}^{-1})(\mathbf{I}_\ell - \gamma_1\mathbf{C}_2\mathbf{A}_{22}^{-1}\mathbf{C}_2^T\mathbf{W}^{-1})\right)(\gamma_1\mathbf{W}^{-1})^{-1}\widehat{\mathbf{S}}^{-1} \\
& = -\left(\mathbf{I}_\ell - (\mathbf{I}_\ell - \mathbf{I}_\ell + (\mathbf{I}_\ell + \gamma_1\mathbf{CA}^{-1}\mathbf{C}^T\mathbf{W}^{-1})^{-1})(\mathbf{I}_\ell - \gamma_1\mathbf{C}_2\mathbf{A}_{22}^{-1}\mathbf{C}_2^T\mathbf{W}^{-1})\right)(\gamma_1\mathbf{W}^{-1})^{-1}\widehat{\mathbf{S}}^{-1} \\
& = -\left(\mathbf{I}_\ell - (\mathbf{I}_\ell + \gamma_1\mathbf{CA}^{-1}\mathbf{C}^T\mathbf{W}^{-1})^{-1}(\mathbf{I}_\ell - \gamma_1\mathbf{C}_2\mathbf{A}_{22}^{-1}\mathbf{C}_2^T\mathbf{W}^{-1})\right)(\gamma_1\mathbf{W}^{-1})^{-1}\widehat{\mathbf{S}}^{-1} \\
& = (\mathbf{I}_\ell - \mathbf{FG})(-\gamma_1\mathbf{W}^{-1})^{-1}\widehat{\mathbf{S}}^{-1}.
\end{aligned}$$

## APPENDIX B. AMG PARAMETERS

The AMG parameter settings used in the numerical experiments are reported in Table B.1.

Parameter	Value
Smoother	Chebyshev
Coarse solver	Amesos-KLU
Smoother sweeps	2
V-cycle applications	1
Aggregation threshold	$10^{-3}$
Max size coarse level	2000

TABLE B.1. Parameters for ML [45] (Trilinos 14.4.0).

## REFERENCES

- [1] F. Alauzet, B. Fabrèges, M. A. Fernández, and M. Landajuela. Nitsche–XFEM for the coupling of an incompressible fluid with immersed thin-walled structures. *Computer Methods in Applied Mechanics and Engineering*, 301:300–335, 2016.
- [2] N. Alshehri, D. Boffi, and C. Chaoeveraprasit. Multigrid Preconditioning for FD-DLM Method in Elliptic Interface Problems. *arXiv:2503.00146*, 2025.
- [3] N. Alshehri, D. Boffi, F. Credali, and L. Gastaldi. Advances on finite element discretization of fluid–structure interaction problems. *Arabian Journal of Mathematics*, 2025.
- [4] N. Alshehri, D. Boffi, and L. Gastaldi. Unfitted mixed finite element methods for elliptic interface problems. *Numerical Methods for Partial Differential Equations*, 40(1):e23063, 2024.
- [5] G. Alzetta and L. Heltai. Multiscale modeling of fiber reinforced materials via non-matching immersed methods. *Computers & Structures*, 239:106334, 2020.
- [6] D. Arndt, W. Bangerth, M. Bergbauer, M. Feder, M. Fehling, J. Heinz, T. Heister, L. Heltai, M. Kronbichler, M. Maier, P. Munch, J.-P. Pelteret, B. Turcksin, D. Wells, and S. Zampini. The deal.II library, version 9.5. *Journal of Numerical Mathematics*, 31(3):231–246, 2023.
- [7] D. Arndt, W. Bangerth, D. Davydov, T. Heister, L. Heltai, M. Kronbichler, M. Maier, J.-P. Pelteret, B. Turcksin, and D. Wells. The deal.II finite element library: Design, features, and insights. *Computers & Mathematics with Applications*, 81:407–422, 2021.
- [8] F. Auricchio, D. Boffi, L. Gastaldi, A. Lefieux, and A. Reali. On a fictitious domain method with distributed Lagrange multiplier for interface problems. *Applied Numerical Mathematics*, 95:36–50, 2015. Fourth Chilean Workshop on Numerical Analysis of Partial Differential Equations (WONAPDE 2013).
- [9] J. W. Barrett and C. M. Elliott. Fitted and unfitted finite-element methods for elliptic equations with smooth interfaces. *IMA Journal of Numerical Analysis*, 7(3):283–300, 1987.

- [10] C. Belponer, A. Caiazzo, and L. Heltai. Mixed-dimensional modeling of vascular tissues with reduced Lagrange multipliers. *arXiv preprint arXiv:2309.06797*, 2025.
- [11] M. Benzi, M. Feder, L. Heltai, and F. Mugnaioni. Scalable augmented Lagrangian preconditioners for fictitious domain problems. *Computer Methods in Applied Mechanics and Engineering*, 450:118522, 2026.
- [12] M. Benzi, G. H. Golub, and J. Liesen. Numerical solution of saddle point problems. *Acta Numerica*, 14:1–137, 2005.
- [13] M. Benzi, E. Haber, and L. Taralli. A preconditioning technique for a class of PDE-constrained optimization problems. *Advances in Computational Mathematics*, 35:149–173, 2011.
- [14] M. Benzi and M. A. Olshanskii. An augmented Lagrangian-based approach to the Oseen problem. *SIAM Journal on Scientific Computing*, 28(6):2095–2113, 2006.
- [15] M. Benzi and M. A. Olshanskii. Field-of-Values convergence analysis of augmented Lagrangian preconditioners for the linearized Navier-Stokes problem. *SIAM Journal on Numerical Analysis*, 49(2):770–788, 2011.
- [16] M. Benzi, M. A. Olshanskii, and Z. Wang. Modified augmented Lagrangian preconditioners for the incompressible Navier-Stokes equations. *International Journal for Numerical Methods in Fluids*, 66(4):486–508, 2011.
- [17] M. Benzi and Z. Wang. Analysis of augmented Lagrangian-based preconditioners for the steady incompressible Navier-Stokes equations. *SIAM Journal on Scientific Computing*, 33(5):2761–2784, 2011.
- [18] S. Bertoluzza, M. Ismail, and B. Maury. Analysis of the fully discrete fat boundary method. *Numerische Mathematik*, 118:49–77, 2011.
- [19] D. Boffi, F. Brezzi, and M. Fortin. *Mixed Finite Element Methods and Applications*. Springer Series in Computational Mathematics. Springer Berlin Heidelberg, 2013.
- [20] D. Boffi, A. Cangiani, M. Feder, L. Gastaldi, and L. Heltai. A comparison of non-matching techniques for the finite element approximation of interface problems. *Computers & Mathematics with Applications*, 151:101–115, 2023.
- [21] D. Boffi, N. Cavallini, and L. Gastaldi. The finite element immersed boundary method with distributed Lagrange multiplier. *SIAM Journal on Numerical Analysis*, 53(6):2584–2604, 2015.
- [22] D. Boffi, F. Credali, and L. Gastaldi. On the interface matrix for fluid-structure interaction problems with fictitious domain approach. *Computer Methods in Applied Mechanics and Engineering*, 401:115650, 2022.
- [23] D. Boffi, F. Credali, and L. Gastaldi. Quadrature error estimates on non-matching grids in a fictitious domain framework for fluid-structure interaction problems. *arXiv:2406.03981*, 2024.
- [24] D. Boffi, F. Credali, and L. Gastaldi. On the stability and conditioning of a fictitious domain formulation for fluid-structure interaction problems. *arXiv preprint arXiv:2505.05228*, 2025.
- [25] D. Boffi, F. Credali, L. Gastaldi, and S. Scacchi. A parallel solver for FSI problems with fictitious domain approach. *Mathematical and Computational Applications*, 28(2):59, 2023.
- [26] D. Boffi, F. Credali, L. Gastaldi, and S. Scacchi. A parallel solver for fluid-structure interaction problems with Lagrange multiplier. *Mathematics and Computers in Simulation*, 220:406–424, 2024.
- [27] E. Burman, S. Claus, P. Hansbo, M. G. Larson, and A. Massing. Cut-FEM: Discretizing geometry and partial differential equations. *International Journal for Numerical Methods in Engineering*, 104(7):472–501, 2015.
- [28] E. Burman, P. Hansbo, and M. Larson. Cut finite element method for divergence-free approximation of incompressible flow: A Lagrange multiplier approach. *SIAM Journal on Numerical Analysis*, 62(2):893–918, 2024.
- [29] E. Burman, P. Hansbo, M. G. Larson, and S. Zahedi. Cut finite element methods. *Acta Numerica*, 34:1–121, 2025.
- [30] P. Causin, J. Gerbeau, and F. Nobile. Added-mass effect in the design of partitioned algorithms for fluid-structure problems. *Computer Methods in Applied Mechanics and Engineering*, 194(42):4506–4527, 2005.
- [31] Y.-C. Chang, T. Hou, B. Merriman, and S. Osher. A level set formulation of Eulerian interface capturing methods for incompressible fluid flows. *Journal of Computational Physics*, 124(2):449–464, 1996.
- [32] L. Chen, H. Wei, and M. Wen. An interface-fitted mesh generator and virtual element methods for elliptic interface problems. *Journal of Computational Physics*, 334:327–348, 2017.
- [33] M. Dauge, A. Düster, and E. Rank. Theoretical and numerical investigation of the finite cell method. *Journal of Scientific Computing*, 65:1039–1064, 2015.
- [34] F. de Prenter, C. Verhoosel, G. van Zwieten, and E. van Brummelen. Condition number analysis and preconditioning of the finite cell method. *Computer Methods in Applied Mechanics and Engineering*, 316:297–327, 2017. Special Issue on Isogeometric Analysis: Progress and Challenges.
- [35] J. Donea, S. Giuliani, and J.-P. Halleux. An arbitrary Lagrangian-Eulerian finite element method for transient dynamic fluid-structure interactions. *Computer Methods in Applied Mechanics and Engineering*, 33(1-3):689–723, 1982.
- [36] A. Ern and J.-L. Guermond. *Theory and Practice of Finite Elements*. Appl. Math. Sci. 159, Springer-Verlag, New York, 2004.
- [37] P. E. Farrell, L. Mitchell, and F. Wechsung. An augmented Lagrangian preconditioner for the 3d stationary incompressible Navier-Stokes equations at high Reynolds number. *SIAM Journal on Scientific Computing*, 41(5):A3073–A3096, 2019.
- [38] W. Garhuom, K. Usman, and A. Düster. An eigenvalue stabilization technique to increase the robustness of the finite cell method for finite strain problems. *Computational Mechanics*, 69(5):1225–1240, 2022.
- [39] R. Glowinski, T.-W. Pan, T. I. Hesla, D. D. Joseph, and J. Periaux. A fictitious domain approach to the direct numerical simulation of incompressible viscous flow past moving rigid bodies: application to particulate flow. *Journal of Computational Physics*, 169(2):363–426, 2001.

- [40] R. Glowinski, T.-W. Pan, and J. Periaux. A Lagrange multiplier/fictitious domain method for the numerical simulation of incompressible viscous flow around moving rigid bodies:(i) case where the rigid body motions are known a priori. *Comptes Rendus de l'Académie des Sciences-Series I-Mathematics*, 324(3):361–369, 1997.
- [41] A. Greenbaum, V. Pták, and Z. Strakoš. Any nonincreasing convergence curve is possible for GMRES. *SIAM Journal on Matrix Analysis and Applications*, 17(3):465–469, 1996.
- [42] M. E. Gurtin, E. Fried, and L. Anand. *The Mechanics and Thermodynamics of Continua*. Cambridge University Press, 2010.
- [43] P. Hansbo, M. G. Larson, and S. Zahedi. A cut finite element method for a Stokes interface problem. *Applied Numerical Mathematics*, 85:90–114, 2014.
- [44] T. Heister and G. Rapin. Efficient augmented Lagrangian-type preconditioning for the Oseen problem using Grad-Div stabilization. *International Journal for Numerical Methods in Fluids*, 71(1):118–134, 2013.
- [45] M. A. Heroux, R. A. Bartlett, V. E. Howle, R. J. Hoekstra, J. J. Hu, T. G. Kolda, R. B. Lehoucq, K. R. Long, R. P. Pawlowski, E. T. Phipps, A. G. Salinger, H. K. Thornquist, R. S. Tuminaro, J. M. Willenbring, A. Williams, and K. S. Stanley. An overview of the Trilinos project. *ACM Transactions on Mathematical Software*, 31(3):397–423, 2005.
- [46] C. W. Hirt, A. A. Amsden, and J. Cook. An arbitrary Lagrangian–Eulerian computing method for all flow speeds. *Journal of Computational Physics*, 14(3):227–253, 1974.
- [47] R. A. Horn and C. R. Johnson. *Matrix Analysis*. Cambridge University Press, 1985.
- [48] T. Hou, X.-H. Wu, and Z. Cai. Convergence of a multiscale finite element method for elliptic problems with rapidly oscillating coefficients. *Mathematics of Computation*, 68(227):913–943, 1999.
- [49] L. Huynh, N. C. Nguyen, J. Peraire, and B. C. Khoo. A high-order hybridizable discontinuous Galerkin method for elliptic interface problems. *International Journal for Numerical Methods in Engineering*, 93(2):183–200, 2013.
- [50] R. Krause and P. Zulian. A parallel approach to the variational transfer of discrete fields between arbitrarily distributed unstructured finite element meshes. *SIAM Journal on Scientific Computing*, 38(3):C307–C333, 2016.
- [51] R.-C. Li. Rayleigh quotient based optimization methods for eigenvalue problems. In *Matrix Functions and Matrix Equations*, Series in Contemporary Applied Mathematics, pages 76–108. World Scientific, 2015.
- [52] R. Löhner and C. Yang. Improved ALE mesh velocities for moving bodies. *Communications in Numerical Methods in Engineering*, 12(10):599–608, 1996.
- [53] D. Malkus. Eigenproblems associated with the discrete LBB condition for incompressible finite elements. *International Journal of Engineering Science*, 19(10):1299–1310, 1981.
- [54] L. Mu, J. Wang, X. Ye, and S. Zhao. A new weak Galerkin finite element method for elliptic interface problems. *Journal of Computational Physics*, 325:157–173, 2016.
- [55] B. Najman and Q. Ye. A minimax characterization for eigenvalues of hermitian pencils. ii. *Linear Algebra and its Applications*, 191:183–197, 1993.
- [56] M. A. Olshanskii and A. Reusken. Grad-div stabilization for Stokes equations. *Mathematics of Computation*, 73:1699–1718, 2004.
- [57] J. W. Pearson, M. Stoll, and A. J. Wathen. Regularization-robust preconditioners for time-dependent PDE-constrained optimization problems. *SIAM Journal on Matrix Analysis and Applications*, 33(4):1126–1152, 2012.
- [58] C. S. Peskin. The immersed boundary method. *Acta Numerica*, 11:479–517, 2002.
- [59] F. Regazzoni. An optimally convergent fictitious domain method for interface problems. *Computer Methods in Applied Mechanics and Engineering*, 431:117327, 2024.
- [60] J. Schöberl. Multigrid methods for a parameter dependent problem in primal variables. *Numerische Mathematik*, 84:97–119, 11 1999.
- [61] J. Schöberl and W. Zulehner. Symmetric indefinite preconditioners for saddle point problems with applications to PDE-constrained optimization problems. *SIAM Journal on Matrix Analysis and Applications*, 29(3):752–773, 2007.
- [62] V. Simoncini. Reduced order solution of structured linear systems arising in certain PDE-constrained optimization problems. *Comput. Optim. Appl.*, 53(2):591–617, Oct. 2012.
- [63] M. Stoll and A. Wathen. All-at-once solution of time-dependent Stokes control. *Journal of Computational Physics*, 232(1):498–515, 2013.
- [64] M. Sussman, P. Smereka, and S. Osher. A level set approach for computing solutions to incompressible two-phase flow. *Journal of Computational Physics*, 114(1):146–159, 1994.
- [65] C. Wang and P. Sun. An augmented Lagrangian Uzawa iterative method for solving double saddle-point systems with semidefinite (2,2) block and its application to DLM/FD method for elliptic interface problems. *Communications in Computational Physics*, 30(1):124–143, 2021.
- [66] Z. Yu. A DLM/FD method for fluid/flexible-body interactions. *Journal of Computational Physics*, 207(1):1–27, 2005.

SCUOLA NORMALE SUPERIORE, PIAZZA DEI CAVALIERI, 7, 56126 PISA, ITALY  
*Email address:* `michele.benzi@sns.it`

DEPARTMENT OF MATHEMATICS, UNIVERSITY OF PISA, LARGO B. PONTECORVO, 5, PISA, 56127, ITALY  
*Email address:* `marco.feder@dm.unipi.it`

DEPARTMENT OF MATHEMATICS, UNIVERSITY OF PISA, LARGO B. PONTECORVO, 5, PISA, 56127, ITALY  
*Email address:* `luca.heltai@unipi.it`

SCUOLA NORMALE SUPERIORE, PIAZZA DEI CAVALIERI, 7, 56126 PISA, ITALY  
*Email address:* `federica.mugnaioni@sns.it`